Solid Earth Discuss., https://doi.org/10.5194/se-2018-50
Manuscript under review for journal Solid Earth
Discussion started: 27 June 2018

Solid Earth Discussions
Open Access
EGU

Influence of basement heterogeneity on the architecture of low subsidence rate Paleozoic intracratonic basins (Ahnet and Mouydir basins, Central Sahara)

Paul Perron[1], Michel Guiraud[1], Emmanuelle Vennin[1], Isabelle Moretti[2], Éric Portier[3], Laetitia Le Pourhiet[4], Moussa Konaté[5]

[1]Université de Bourgogne Franche-Comté, Centre des Sciences de la Terre, UMR CNRS 6282 Biogéosciences, 6 Bd Gabriel, 21000 Dijon, France.

[2]ENGIE, Département Exploration & Production, 1, place Samuel de Champlain, Faubourg de l'Arche, 92930 Paris La Défense, France.

[3]NEPTUNE Energy International S.A., 9-11 Allée de l'Arche – Tour EGEE – 92400 Courbevoie, France.

[4]Sorbonne Université, CNRS-INSU, Institut des Sciences de la Terre Paris, ISTeP UMR 7193, F-75005 Paris, France.

[5]Département de Géologie, Université Abdou Moumouni de Niamey, BP :10662, Niamey, Niger.

Corresponding author: paul.perron@u-bourgogne.fr, paul.perron@hotmail.fr

Abstract

The Paleozoic intracratonic North African Platform is characterized by an association of arches (ridges, domes, swells or paleo-highs) and low subsidence rate syncline basins of different wavelengths (75–620 km). The structural framework of the platform results from the accretion of Archean and Proterozoic terranes during the Pan-African orogeny (750–580 Ma). The Ahnet and Mouydir basins are successively delimited from east to west by the Amguid El Biod, Arak-Foum Belrem, and Azzel Matti arches, bounded by inherited Precambrian sub-vertical fault systems which were repeatedly reactivated or inverted during the Paleozoic.

Solid Earth Discuss., https://doi.org/10.5194/se-2018-50
Manuscript under review for journal Solid Earth
Discussion started: 27 June 2018

Major unconformities are related to several tectonic events such as the Cambrian–Ordovician extension, Ordovician–Silurian glacial rebound, Silurian–Devonian "Caledonian" extension/compression, late Devonian extension/compression, and "Hercynian" compression. The deposits associated with these arches and syncline basins exhibit thickness variations and facies changes ranging from continental to marine environments. The arches are characterized by thin amalgamated deposits with condensed and erosional surfaces, whereas the syncline basins exhibit thicker and well-preserved successions. In addition, the vertical facies succession evolves from thin Silurian to Givetian deposits into thick Upper Devonian sediments. Synsedimentary deformations are evidenced by wedges, truncations, and divergent onlaps. Locally, deformation is characterized by near-vertical planar normal faults responsible for horst and graben structuring associated with folding during the Cambrian–Ordovician–Silurian period. These structures may have been inverted or activated during the Devonian compression and the Carboniferous. The sedimentary infilling pattern and the nature of deformation result from the slow Paleozoic reactivation of Precambrian terranes bounded by vertical lithospheric fault zones. Alternating periods of tectonic quiescence and low-rate subsidence acceleration associated with extension and local inversion tectonics correspond to a succession of Paleozoic geodynamic events (i.e. far-field orogenic belt, glaciation).

Keywords: intracratonic basin, Paleozoic, arches, low-rate subsidence, tectonic heritage, terranes, Central Sahara

1 Introduction

Paleozoic deposits fill numerous intracratonic basins, which may also be referred to as "cratonic basins", "interior cratonic basins", or "intracontinental sags". Intracratonic basins are widespread around the world (see Fig. 6 from Heine et al., 2008) and exploration for non-conventional petroleum has revived interest in them. They are located in "stable" lithospheric

areas and share several common features (see Allen and Armitage, 2011 and references therein) such as their geometries (i.e. large circular, elliptical, saucer-shaped to oval), their stratigraphy (i.e. filled with continental to shallow-water sediments), their low rate of sedimentation (an average of 7 m/Myr), their long-term subsidence (sometimes more than 540 Myr), and their structural framework (reactivation of structures and emergence of arches also referred to in the literature as "ridges", "paleo-highs", "domes", and "swells"). Multiple hypotheses and models have been proposed to explain how these slowly subsiding, long-lived intracratonic basins formed and evolved (see Allen and Armitage, 2011 and references therein or Hartley and Allen, 1994). However, their tectonic and sedimentary architectures are often poorly constrained.

The main specificities of intracratonic basins are found on the Paleozoic North Saharan Platform. The sedimentary infilling during c. 250 Myr is relatively thin (i.e. around a few hundred to a few thousand meters), of great lateral extent (i.e. 16 million km^2), and is separated by major regional unconformities (Beuf et al., 1971; Carr, 2002; Eschard et al., 2005, 2010; Fabre, 1988, 2005; Fekirine and Abdallah, 1998; Guiraud et al., 2005; Legrand, 2003). Depositional environments were mainly continental to shallow-marine and homogeneous. Very slow and subtle lateral variations occurred over time (Beuf et al., 1971; Carr, 2002; Fabre, 1988; Guiraud et al., 2005; Legrand, 2003). The Paleozoic North Saharan Platform is arranged (Fig. 1) into an association of long-lived broad synclines (i.e. basins) and anticlines (i.e. arches swells, domes, highs, or ridges) of different wavelengths (λ: 75–620 km). Burov and Cloetingh, (2009) report deformation wavelengths of the order of 200–600 km when the whole lithosphere is involved and of 50–100 km when the crust is decoupled from the lithospheric mantle. This insight suggests that the inherited basement fabric influences basin architecture at a large scale. Intracratonic basins are affected by basement involved faults which are often reactivated in response to tectonic pulses (Beuf et al., 1971;

Solid Earth Discuss., https://doi.org/10.5194/se-2018-50
Manuscript under review for journal Solid Earth
Discussion started: 27 June 2018

74 Boote et al., 1998; Eschard et al., 2010; Fabre, 1988; Frizon de Lamotte et al., 2013; Galeazzi
75 et al., 2010; Guiraud et al., 2005; Wendt et al., 2006).

76 In this study of the Ahnet and Mouydir basins, a multidisciplinary workflow involving
77 various tools (e.g. seismic profiles, satellite images) and techniques (e.g. photo-geology,
78 seismic interpretation, well correlation, geophysics, geochronology) has enabled us to (1)
79 make a tectono-sedimentary analysis, (2) determine the spatial arrangement of depositional
80 environments calibrated by biostratigraphic zonation, (3) characterize basin geometry, and (4)
81 ascertain the inherited architecture of the basement and its tectonic evolution. We propose a
82 conceptual coupled model explaining the architecture of the intracratonic basins of the North
83 Saharan Platform. This model highlights the role of basement heritage heterogeneities in an
84 accreted mobile belt and their influence on the structure and evolution of intracratonic basins.
85 It is a first step towards a better understanding of the factors and mechanisms that drive
86 intracratonic basins.

87 ## 2 Geological setting: The Paleozoic North Saharan Platform and the Ahnet and
88 Mouydir basins

89 The Ahnet and Mouydir basins (Figs 1 and 3) are located in south-western Algeria, north-
90 west of the Hoggar massif (Ahaggar). They are N–S oval depressions filled by Paleozoic
91 deposits. The basins are bounded to the south by the Hoggar massif (Tuareg Shield), to the
92 west by the Azzel Matti arch, to the east by the Amguid El Biod arch and they are separated
93 by the Arak-Foum Belrem arch.

94 Figure 2 synthetizes the lithostratigraphy, the large-scale sequence stratigraphic framework
95 delimited by five main regional unconformities (A to E), and the tectonic events proposed in
96 the literature (cf. references under Fig. 2) affecting the Paleozoic North Saharan Platform.

Solid Earth Discuss., https://doi.org/10.5194/se-2018-50
Manuscript under review for journal Solid Earth
Discussion started: 27 June 2018

During the Paleozoic, the Ahnet and Mouydir basins were part of a set of the super-continent Gondwana (Fig. 1). This super-continent resulted from the collision of the West African Craton (WAC) and the East Saharan Craton (ESC), sandwiching the Tuareg Shield (TS) mobile belt during the Pan-African orogeny (Craig et al., 2006; Guiraud et al., 2005; Trompette, 2000). This orogenic cycle followed by the chain's collapse (c. 1000–525 Ma) was also marked by phases of oceanization and continentalization (c. 900–600 Ma) giving rise to the heterogeneous terranes in the accreted mobile belt (e.g. Trompette, 2000). Then, there is evidence of a complex and polyphased history throughout the Paleozoic (Fig. 2), with alternating periods of quiescence and tectonic activity, individualizing and rejuvenating ancient NS, NE–SW, or NW–SE structures in arch and basin configurations (Badalini et al., 2002; Bennacef et al., 1971; Beuf et al., 1968a, 1971; Boote et al., 1998; Boudjema, 1987; Chavand and Claracq, 1960; Coward and Ries, 2003; Craig et al., 2006; Eschard et al., 2005, 2010, Fabre, 1988, 2005; Frizon de Lamotte et al., 2013; Guiraud et al., 2005; Logan and Duddy, 1998; Lüning, 2005; Wendt et al., 2006). The Paleozoic successions of the North Saharan Platform are predominantly composed of siliciclastic detrital sediments (Beuf et al., 1971; Eschard et al., 2005). They form the largest area of detrital sediments ever found on continental crust (Burke et al., 2003), dipping gently NNW (Beuf et al., 1969, 1971; Fabre, 1988, 2005; Fröhlich et al., 2010; Gariel et al., 1968; Le Heron et al., 2009). Carbonate deposits are observed from the Mid–Late Devonian to the Carboniferous (Wendt, 1995, 1988, 1985; Wendt et al., 2009b, 2006, 1997, 1993; Wendt and Kaufmann, 1998). From south to north, the facies progressively evolve from continental fluviatile to shallow marine (i.e. upper to lower shoreface) and then to offshore facies (Beuf et al., 1971; Carr, 2002; Eschard et al., 2005, 2010, Fabre, 1988, 2005; Fekirine and Abdallah, 1998; Guiraud et al., 2005; Legrand, 1967a).

3 Data and methods

122 A multidisciplinary approach has been used in this study integrating new data in particular
123 from the Ahnet and Mouydir basins (see supplementary data 1):

124 - Geographic Information System analysis (GIS);

125 - The basins and the main geological structures were identified from Landsat satellite images;

126 - Seismic section interpretation;

127 - Sedimentological and well-log analysis;

128 - Biostratigraphy and sequence stratigraphy;

129 - Geochronology and geophysical data.

130 The Paleozoic series of the Ahnet and Mouydir basins are well-exposed over an area of
131 approximately 170,000 km^2 and are well observed in satellite images (Google Earth and
132 Landsat from USGS). Furthermore, a significant geological database (i.e. wells, seismic
133 records, field trips, geological reports) has been compiled in the course of petroleum
134 exploration since the 1950s. The sedimentological dataset is based on the integration and
135 analysis of cores, outcrops, well-logs, and of lithological and biostratigraphic data. Facies
136 described from cores and outcrops of these studies were grouped into facies associations
137 corresponding to the main depositional environments observed on the Saharan Platform (table
138 1). Characteristic gamma-ray patterns (electrofacies) are proposed to illustrate the different
139 facies associations. The gamma-ray (GR) peaks are commonly interpreted as the maximum
140 flooding surfaces (MFS) (e.g. Catuneanu et al., 2009; Galloway, 1989; Milton et al., 1990;
141 Serra, 2009). Time calibration of well-logs and outcrops is based on palynomorphs
142 (essentially Chitinozoans and spores), conodonts, goniatites, and brachiopods (Wendt et al.,
143 2006).

Solid Earth Discuss., https://doi.org/10.5194/se-2018-50
Manuscript under review for journal Solid Earth
Discussion started: 27 June 2018

144 Synsedimentary extensional and compressional markers are characterized in this structural
145 framework based on the analyses of satellite images (Figs 4 and 5), seismic profiles (Fig. 6),
146 21 wells (W1 to W21), and 12 outcrop cross-sections (O1 to O12). Wells and outcrop sections
147 are arranged into three E–W sections (Figs 9, 10 and supplementary data 2) and one N–S
148 section (supplementary data 3). Satellite images (Figs 4 and 5) and seismic profiles (Fig. 6)
149 are located at key areas (i.e. near arches) illustrating the relevant structures (Fig. 3). The
150 calibration of the key stratigraphic horizon on seismic profiles (Figs 9 and 10) was settled by
151 sonic well-log data using PETREL and OPENDTECT software. Nine key horizons easily
152 extendable at the regional scale are identified and correspond to major unconformities: top
153 Infra-Cambrian, top Ordovician, top Silurian, top Pragian, top Givetian, top mid-Frasnian, top
154 Famennian, top Quaternary and top Hercynian unconformities (Figs 9 and 10). The
155 stratigraphic layers are identified by the integration of satellite images (Google Earth and
156 Landsat USGS: https://earthexplorer.usgs.gov/) and the 1:20,000 geological map of Algeria
157 (Bennacef et al., 1974; Bensalah et al., 1971).

158 Subsidence analysis characterizes the vertical displacements of a given sedimentary
159 depositional surface by tracking its subsidence and uplift history (Van Hinte, 1978). The
160 resulting curve details the total subsidence history for a given stratigraphic column (Allen and
161 Allen, 2005; Van Hinte, 1978). Backstripping is also used to restore the initial thicknesses of
162 a sedimentary column (Allen and Allen, 2005; Angevine et al., 1990). Lithologies and
163 paleobathymetries have been defined using facies analysis or literature data. Porosity and the
164 compaction proxy are based on experimental data from Sclater and Christie, (1980). In this
165 study, subsidence analyses were performed on sections using OSXBackstrip software
166 performing 1D Airy backstripping (after Allen and Allen, 2005; Watts, 2001; available at:
167 http://www.ux.uis.no/nestor/work/programs.html).

168 **4 Structural framework and tectono-sedimentary structure analyses**

Solid Earth Discuss., https://doi.org/10.5194/se-2018-50
Manuscript under review for journal Solid Earth
Discussion started: 27 June 2018

The structural architecture of the North Saharan Platform (Fig. 1) is characterized by an association of syncline basins and anticlines (i.e. arches, domes, etc.). The basins (or sub-basins) are mostly circular to oval. They are bounded by arches which correspond to the mainly N–S Azzel-Matti, Arak-Foum Belrem, Amguid El Biod, and Tihemboka arches, the NE–SW Bou Bernous, Ahara, and Gargaf arches, and the NW–SE Saoura and Azzene arches (Fig. 1). The basins are structured by major faults frequently associated with broad asymmetrical folds displayed by three main trends (Fig. 1): (1) near-N–S, varying from N0° to N10° or N160°, (2) from N40° to 60°, and (3) N100° to N140° directions (Figs 1, 3A, and 4). These fault zones are about 100 km (e.g. faults F1 and F2, Fig. 4) to tens of kilometers lengths (e.g. faults F3 to F8, Fig. 4).

4.1 Synsedimentary extensional markers

Extensional markers are characterized by the settlement of steeply west- or eastward-dipping basement normal faults associated with colinear syndepositional folds of several kilometers in length (e.g. Fig. 5A-A', 5B-B', 5C-C', 5E-E' and 6A), represented by footwall anticline and hanging wall syncline-shaped forced folds. They are located in the vicinity of different arches (Fig. 3) such as the Tihemboka arch (Figs 4BB', 5A-A' and 5B-B'), Arak-Foum Belrem arch (Figs 4A-A', 5C-C' to 5F-F' and 6A, 6C), Azzel Matti arch (Fig. 6B), and Bahar El Hamar area intra-basin arch (Fig. 6D). These tectonic structures can be featured by basement blind faults (e.g. fault F5 in Fig. 5C-C', fault F1 in Figs 5D-D', 5F-F', and 6A). The deformation pattern is mainly characterized by brittle faulting in Cambrian–Ordovician series down to the basement and fault-damping in Silurian series (e.g. fault F2 in Fig. 5AA', faults F1 to F6 in Fig. 6B). The other terms of the series (i.e. Silurian to Carboniferous) are usually affected by folding except (see F1 faults in Figs 5F-F', 6B, 6D and 6C) where the brittle deformation can be propagated to the Upper Devonian (due to reactivation and/or inversion as suggested in the next paragraph).

Solid Earth Discuss., https://doi.org/10.5194/se-2018-50
Manuscript under review for journal Solid Earth
Discussion started: 27 June 2018

194 In association with the extensional markers, thickness variations and tilted divergent onlaps of
195 the sedimentary series (i.e. wedge-shaped units, progressive unconformities) in the hanging
196 wall syncline of the fault escarpments are observed (Figs 5 and 6). These are attested using
197 photogeological analysis of satellite images (Fig. 5) and are marked by a gentler dip angle of
198 the stratification planes away from the fault plane (i.e. fault core zone). The markers of
199 syndepositional deformation structures are visible in the hanging-wall synclines of
200 Precambrian to Upper Devonian series (Figs 5 and 6).

201 The footwall anticline and hanging-wall syncline-shaped forced folds recognized in this study
202 are very similar to those described in the literature by Schlische (1995), Withjack et al. (1990,
203 2002), Withjack and Callaway (2000), Khalil and McClay (2002), and Grasemann et al.
204 (2005). The wedge-shaped units (DO0 to DO3; Figs 4, 5 and 6) associated with the hanging-
205 wall synclines are interpreted as synsedimentary normal fault-related folding. The whole
206 tectonic framework forms broad extensional horsts and graben related to synsedimentary
207 forced folds controlling basin shape and sedimentation (Figs 4, 5 and 6).

208 Following Khalil and McClay (2002), Lewis et al. (2015), Shaw et al. (2005), and Withjack et
209 al. (1990), we use the ages of the growth strata (i.e. wedge-shaped units) to determine the
210 timing of the deformation. The main four wedge-shaped units identified (DO0 to DO3) are
211 indicative of the activation and/or reactivation of the normal faults (extensional settings)
212 during Neoproterozoic, Cambrian–Ordovician, Early to Mid Silurian and Mid to Late
213 Devonian times.

214 In planar view, straight (F1 in Fig. 4A-A') and sinuous faults (F2, F3, F3', F4, F4', and F5 in
215 Fig. 4AA') can be identified. The sinuous faults are arranged "en echelon" into several
216 segments with relay ramps. These faults are 10 to several tens of kilometers long with vertical
217 throws of hundreds of meters that fade rapidly toward the fault tips. The sinuous geometry of

normal undulated faults as well as the rapid lateral variation in fault throw are controlled by the propagation and the linkage of growing parent and tip synsedimentary normal faults (Marchal et al., 2003, 1998; Fig. 4A-A').

According to Holbrook and Schumm (1999), river patterns are extremely sensitive to tectonic structure activity. Here we find that the synsedimentary activity of the extensional structures is also evidenced by the influence of the fault scarp on the distribution and orientation of sinuous channelized sandstone body systems (dotted red lines in Fig. 4B-B').

4.2 Synsedimentary compressional markers (inversion tectonics)

After the development of the extensional tectonism described previously, evidence of synsedimentary compressional markers can be identified. These markers are located and preferentially observable near the Arak-Foum Belrem arch (Fig. 5F-F', F2 in Fig. 6C), the Azzel Matti arch (2 in Figs 6B), and the Bahar El Hamar area intra-basin arch (2 in Fig. 6D). The tectonic structures take the form of inverse faulting reactivating former basement faults (F1' in Fig. 5F-F', F1 in Fig. 6C, F1' in Fig. 6D, F1 in Fig. 6B). The synsedimentary inverse faulting is demonstrated by the characterization of asymmetric anticlines especially observable in satellite images and restricted to the fault footwalls (Figs 4A-A' along F1-F2).

Landsat image analysis combined with the line drawing of certain seismic lines reveals several thickness variations reflecting divergent onlaps (i.e. wedge-shaped units) which are restricted to the hanging-wall asymmetric anticlines (2 in Figs 5F-F', 6B, 6C and 6D). The compressional synsedimentary markers clearly post-date extensional divergent onlaps at hanging-wall syncline-shaped forced folds (1 in Figs 6B, 6C and 6D). This architecture is very similar to classical positive inversion structures of former inherited normal faults (Bellahsen and Daniel, 2005; Bonini et al., 2012; Buchanan and McClay, 1991; Ustaszewski et al., 2005). Tectonic transport from the paleo-graben hanging-wall toward the paleo-horst

Solid Earth Discuss., https://doi.org/10.5194/se-2018-50
Manuscript under review for journal Solid Earth
Discussion started: 27 June 2018

footwall (F1, F2-F2', F4-F4' in Fig. 6B; F1-F1' in Fig. 6B) is evidenced. Further positive tectonic inversion architecture is identified by tectonic transport from the paleo-horst footwall to the paleo-graben hanging wall (F1-F1' in Fig. 5F-F'; F1, F5, and F6 in Fig. 6C). This second type of tectonic inversion is very similar to the transported fault models defined by Butler (1989) and Madritsch et al. (2008). The local positive inversions of inherited normal faults occurred during Silurian–Devonian (F4' Fig. 6B) and Mid to Late Devonian times (Figs 6B, 6C and 6D). A late significant compression event between the end of the Carboniferous and the Early Mesozoic was responsible for the exhumation and erosion of the tilted Paleozoic series. This series is related to the Hercynian angular unconformity surface (Fig. 6B).

5 Stratigraphy and sedimentology

The whole sedimentary series described in the literature is composed of fluviatile Cambrian (Beuf et al., 1968a, 1968b, 1971; Eschard et al., 2005, 2010), glacial Ordovician (Beuf et al., 1968a, 1968b, 1971; Eschard et al., 2005, 2010), argillaceous deep marine Silurian (Eschard et al., 2005, 2010; Legrand, 1986, 1996; Lüning et al., 2000) and offshore to embayment Carboniferous (Wendt et al., 2009) deposits. In this complete sedimentary succession, we have focused on the Devonian deposits as they are very sensitive to and representative of basin dynamics. The architecture of the Devonian deposits allows us to approximate the main forcing factors controlling the sedimentary infilling of the basin and its synsedimentary deformation. Nine facies associations organized into four depositional environments are defined to reconstruct the architecture and the lateral and vertical sedimentary evolution of the basins (Figs 9, 10, supplementary data 2 and 3).

5.1 Facies association, depositional environments, and erosional unconformities

Based on the compilation and synthesis of internal studies (Eschard et al., 1999), published papers on the Algerian platform (Beuf et al., 1971; Eschard et al., 2010, 2005; Henniche, 2002) and on the Ahnet and Mouydir basins (Biju-Duval et al., 1968; Wendt et al., 2006) plus the present study, eleven main facies associations (AF1 to AF5) and four depositional environments are proposed for the Devonian succession (table 1). They are associated with their gamma-ray responses (Figs 7 and 8). They are organized into two continental/fluvial (AF1 to AF2), four transitional/coastal plain (AF3a to AF3d), three shoreface (AF4a to AF4c), and two offshore (AF5a to AF5b) sedimentary environments.

5.1.1 Continental fluvial environments

This depositional environment features the AF1 (fluvial) and the AF2 (flood plain) facies association (Table 1). Facies association AF1 is mainly characterized by a thinning-up sequence with a basal erosional surface and trough cross-bedded intraformational conglomerates with mud clast lag deposits, quartz pebbles, and imbricated grains (Table 1). It passes into medium to coarse trough cross-bedded sandstones, planar cross-bedded siltstones, and laminated shales. These deposits are associated with rare bioturbations (expect at the surface of the sets), ironstones, phosphorites, corroded quartz grains, and phosphatized pebbles. Laterally, facies association AF2 is characterized by horizontally laminated and very poorly sorted silt to argillaceous fine sandstones. They contain frequent root traces, plant debris, well-developed paleosols, bioturbations, nodules, and ferruginous horizons. Current ripples and climbing ripples are associated in prograding thin sandy layers.

In AF1, the basal erosional reworking and high energy processes are characteristic of channel-filling of fluvial systems (Allen, 1983; Owen, 1995). Eschard et al. (1999) identify three fluvial systems (see A, B, and C in Fig. 8) in the Tassili-N-Ajjers outcrops: braided dominant (AF1a), meandering dominant (AF1b), and straight dominant (AF1c). They differentiate them

by their different sinuosity, directions of accretion (lateral or frontal), the presence of mud drapes, bioturbations, and giant epsilon cross-bedding. Gamma-ray signatures of these facies associations (A, B, and C in Fig. 8) are cylindrical with an average value of 20 gAPI. The gamma ray shapes are largely representative of fluvial environments (Rider, 1996; Serra, 2009; Wagoner et al., 1990). The bottom is sharp with high value peaks and the tops are frequently fining-up, which may be associated with high values caused by argillaceous flood plain deposits and roots (Eschard et al., 1999). AF2 is interpreted as humid floodplain deposits (Allen, 1983; Owen, 1995) with crevasse splays or preserved levees of fluvial channels (Eschard et al., 1999). Gamma-ray curves of AF2 (D, Fig. 8) show a rapid succession of low to very high peak values, ranging from 50 to 200 gAPI. AF1 and AF2 are typical of the Pragian "Oued Samene" Formation (Wendt et al., 2006). In the Illizi basin, these facies are mainly recorded in the Cambrian Ajjers Formation and the Lochkovian to Pragian "Middle Barre" and "Upper Barre" Formations (Beuf et al., 1971; Eschard et al., 2005).

5.1.2 Transitional coastal plain environments

This depositional environment comprises facies associations AF3a (delta/estuarine), AF3b (fluvial/tidal distributary channels), AF3c (tidal sand flat), AF3d (lagoon/mudflat) (table 1). AF3a is mainly dominated by sigmoidal cross-bedded heterolithic rocks with mud drapes. It is also characterized by fine to coarse, poorly sorted sandstones and siltstones often structured by combined flow ripples, flaser bedding, wavy bedding, and some rare planar bedding. Mud clasts, root traces, desiccation cracks, water escape features, and shale pebbles are common. The presence of epsilon bedding is attested, which is formed by lateral accretion of a river point bar (Allen, 1983). The bed surface sets are intensively bioturbated (*Skolithos* and *Planolites*) indicating a shallow marine subtidal setting (Pemberton and Frey, 1982). Faunas such as brachiopods, trilobites, tentaculites, and graptolites are present. AF3b exhibits a

Solid Earth Discuss., https://doi.org/10.5194/se-2018-50
Manuscript under review for journal Solid Earth
Discussion started: 27 June 2018

fining-up sequence featured by a sharp erosional surface, trough cross-bedded, very coarse-grained, poorly sorted sandstone at the base and sigmoidal cross-bedding at the top (Figs 7 and 8). AF3c is formed by fine-grained to very coarse-grained sigmoidal cross-bedded heterolithic sandstones with multidirectional tidal bundles. They are also structured by lenticular, flaser bedding and occasional current and oscillation ripples with mud cracks. They reveal intense bioturbation composed of *Skolithos* (Sk), *Thalassinoides* (Th), and *Planolites* (Pl) ichnofacies indicating a shallow marine subtidal setting (Frey et al., 1990; Pemberton and Frey, 1982). AF4d is characterized by horizontally laminated mudstones associated with varicolored shales and fine-grained sandstones. They exhibit mud cracks, occasional wave ripples, and rare multidirectional current ripples. These sedimentary structures are poorly preserved because of intense bioturbation composed of *Skolithos* (Sk), *Thalassinoides* (Th), and *Planolites* (Pl). Fauna includes ammonoids (rare), goniatites, calymenids, pelecypod molds, and brachiopod coquinas.

In AF3a, both tidal and fluvial systems in the same facies association can be interpreted as an estuarine system (Dalrymple et al., 1992; Dalrymple and Choi, 2007). The gamma-ray signature is characterized by a convex bell shape with rapidly alternating low to high values (30 to 60 gAPI) due to the mud draping of the sets (see E Fig. 8). These forms of gamma ray are typical of fluvial-tidal influenced environments with upward-fining parasequences (Rider, 1996; Serra, 2009; Wagoner et al., 1990). AF3a is identified at the top of the Pragian "Oued Samene" Formation and in Famennian "Khenig" Formation (Wendt et al., 2006) in the Ahnet and Mouydir basins. In the Illizi basin, AF3a is mostly recorded at the top Cambrian of the Ajjers Formation, in the Lochkovian "Middle bar", and at the top Pragian of the "Upper bar" Formation (Beuf et al., 1971; Eschard et al., 2005). The AF3b association can be characterized by a mixed fluvial and tidal dynamic based on criteria such as erosional basal contacts, fining-upward trends or heterolythic facies (Dalrymple et al., 1992; Dalrymple and

Choi, 2007). They are associated with abundant mud clasts, mud drapes, and bioturbation indicating tidal influences (Dalrymple et al., 2012, 1992; Dalrymple and Choi, 2007). The major difference with the estuarine facies association (AF3a) is the slight lateral extent of the channels which are only visible in outcrops (Eschard et al., 1999). The gamma-ray pattern is very similar to the estuarine electrofacies (see F Fig. 8). AF3c is interpreted as a tidal sandflat laterally present near a delta (Lessa and Masselink, 1995) and associated with an estuarine environment (Leuven et al., 2016). The gamma-ray signature (see G Fig. 8) is distinguishable by its concave funnel shape with alternating low and high peaks (25 to 60 gAPI) due to the heterogeneity of the deposits and rapid variations in the sand/shale ratio. These facies are observed in the "Tigillites Talus" Formation of the Illizi basin (Eschard et al., 2005). In AF4d, both ichnofacies and facies are indicative of tidal mudflat/lagoonal depositional environments (Dalrymple et al., 1992; Dalrymple and Choi, 2007; Frey et al., 1990). The gamma-ray signature has a distinctively high value (80 to 130 gAPI) and an erratic shape (see H Fig. 8). AF4d is observed in the "Atafaitafa" Formation and in the Emsian prograding shoreface sequence of the Illizi basin (Eschard et al., 2005). It is also recorded in the Lochkovian "Oued Samene" Formation and the Famennian "Khenig" Sandstones (Wendt et al., 2006).

5.1.3 Shoreface environments

This depositional environment is composed of AF4a (subtidal), AF4b (upper shoreface), and AF4c (lower shoreface) facies associations (Table 1). AF4a is characterized by the presence of brachiopods, crinoids, and diversified bioturbations, by the absence of emersion, and by the greater amplitude of the sets in a dominant mud lithology (Eschard et al., 1999). AF4b is heterolithic and composed of fine to medium-grained sandstones (brownish) interbedded with argillaceous siltstones and bioclastic carbonated sandstones. Sedimentary structures include oscillation ripples, swaley cross-bedding, flaser bedding, cross-bedding, convolute bedding, wavy bedding, and low-angle planar cross-stratification. Sediments were affected by

364 moderate to highly diversified bioturbation by *Skolithos* (Sk), *Cruziana*, *Planolites*, (Pl)
365 *Chondrites* (Ch), *Teichichnus* (Te), *Spirophytons* (Sp) and are composed of ooids, crinoids,
366 bryozoans, stromatoporoids, tabulate and rugose corals, pelagic styliolinids, neritic
367 tentaculitids, and brachiopods. AF4c can be distinguished by a low sand/shale ratio, thick
368 interbeds, abundant HCS, deep groove marks, slumping, and intense bioturbation (Table 1).

369 AF4a is interpreted as a lagoonal shoreface. The gamma-ray pattern (see I Fig. 8) is
370 characterized by a concave bell shape influenced by a low sand/shale ratio with values
371 fluctuating between 100 and 200 gAPI. AF4a is identified in the "Tigillites Talus" Formation
372 and the Emsian sequence of the Illizi basin (Eschard et al., 2005) and in the Lochkovian
373 "Oued Samene" Formation (Wendt et al., 2006). AF4b is interpreted as a shoreface
374 environment. The presence of swaley cross-bedding produced by the amalgamation of storm
375 beds (Dumas and Arnott, 2006) and other cross-stratified beds is indicative of upper shoreface
376 environments (Loi et al., 2010). The gamma-ray pattern (see J and K Fig. 8) displays concave
377 erratic egg shapes with a very regularly decreasing-upward trend and ranging from offshore
378 shale with high values (80 to 60 gAPI) to clean sandstone with low values at the top (40 to 60
379 gAPI). AF4b is observed in the "Atafaitafa" Formation corresponding to the "Passage zone"
380 Formation of the Illizi basin (Eschard et al., 2005). AF4c is interpreted as a lower shoreface
381 environment (Dumas and Arnott, 2006; Suter, 2006). The gamma-ray pattern displays the
382 same features as the upper shoreface deposits with lower values (i.e. muddier facies) ranging
383 from 100 to 80 gAPI (see J and K Fig. 8).

384 **5.1.4 Offshore marine environments**

385 This depositional environment is composed of AF5a and AF5b facies associations (table 1).
386 AF5a is mainly defined by wavy to planar-bedded heterolithic silty-shales interlayered with
387 fine-grained sandstones. It also contains bundles of skeletal wackestones and calcareous

mudstones. The main sedimentary structures are lenticular sandstones, rare hummocky cross-bedding, mud mounds, low-angle cross-bedding, tempestite bedding, slumping, and deep groove marks. Sediments can present rare horizontal bioturbation such as *Zoophycos* (Z), *Teichichnus* (Te), and *Planolites* (Pl). AF5b is characterized by an association of black silty shales with occasional bituminous wackestones and packstones. It is composed of graptolites, gonitaties, orthoconic nautiloids, pelagic pelecypods, limestone nodules, tentaculitids, ostracods, and rare fish remains. Rare bioturbation such as *Zoophycos* (Z) is visible.

In AF5a, the occurrence of HCS, the decrease in sand thickness and grain size together with the fossil traces indicate a deep marine environment under the influence of storms (Aigner, 1985; Reading, 2002). The gamma-ray pattern is serrated and erratic with values well grouped around high values from 120 to 140 gAPI (see L Fig. 8). Positive peaks may indicate siltstone to sandstone ripple beds. AF5b is interpreted as lower offshore deposits (Aigner, 1985; Stow and Piper, 1984; Stow et al., 2001). Here again the gamma-ray signature is serrated and erratic with values well grouped around 140 gAPI (see L Fig. 8). Hot shales with anoxic conditions are characterized by gamma-ray peaks (>140 gAPI). These gamma-ray patterns are typical of offshore environments dominated by shales (Rider, 1996; Serra, 2009; Wagoner et al., 1990). AF5a and AF5b are observed in the Silurian "Graptolites shales" Formation and the Emsian "Orsine" Formation of the Illizi basin (Beuf et al., 1971; Eschard et al., 2005; Legrand, 1996, 1986). The "Meden Yahia" and "Termatasset" Shales have the same facies (Wendt et al., 2006).

5.2 Sequential framework and unconformities

The high-resolution facies analysis, depositional environments, stacking patterns, and surface geometries observed in the Paleozoic succession reveal at least two different orders of depositional sequences (large and medium scale, Fig. 7) considered as

transgressive/regressive T/R (e.g. Catuneanu et al., 2009). The sequential framework proposed in Fig. 7B result from the integration of the vertical evolution the main surfaces (Fig. 7A) and the gamma-ray pattern (Fig. 8). The Devonian series under focus exhibits nine medium-scale sequences (D1 to D9, Fig. 7; Figs 9, 10, supplementary data 2 and 3) bounded by 10 major sequence boundaries (HD0 to HD9), and nine major flooding surfaces (MFS1 to MFS9). The correlation of the different sequences at the scale of the different basins and arches is used to build two E–W (Figs 9, 10, supplementary data 2) and one N–S (supplementary data 3) cross-sections.

The result of the analysis of the general pattern displayed by the successive sequences reveal two major patterns (Figs 9 and 10) limited by a major flooding surface MFS5. The first pattern extends from the Oued Samene to Adrar Morrat Formations and is dated from the Lochkovian to Givetian. D1 to D5 medium-scale sequences indicate a general proximal clastic depositional environment (dominated by fluvial to transitional and shoreface facies) with intensive lateral facies evolution. This first pattern is thin (from 500 m in the basin depocenter to 200 m around the basin rim) and with successive amalgamated surfaces on the edge of the arches between the “Passage zone” and “Oued Samene” Formations (Figs 5C-C’, 6A, 6C, 6D, and 9). It is delimited at the bottom by the HD0 surface corresponding to the Silurian/Devonian boundary. D1 to D3 are composed of T-R sequences with a first deepening transgressive trend indicative of a transition from continental to marine deposits bounded by a major MFS and evolving into a second shallowing trend from deep marine to shallow marine depositional environments. D1 to D3 thin progressively toward the edge and the continental deposits, in the central part of the basin, pass laterally into a major unconformity. The amalgamation of the surfaces and rapid lateral variations of facies between the Ahnet basin and Azzel Matti and Arak-Foum Belrem arches demonstrate a tectonic control related to the presence of subsiding basins and paleo-highs (i.e. arches).

Solid Earth Discuss., https://doi.org/10.5194/se-2018-50
Manuscript under review for journal Solid Earth
Discussion started: 27 June 2018

D4 and D5 display the same T-R pattern with a reduced continental influence and upward decrease in lateral facies variations and thicknesses. The D5 sequence is mainly composed of shoreface carbonates. Evidence of mud mounds preferentially located along faults are well-documented in the area for that time (Wendt et al., 2006, 1997, 1993; Wendt and Kaufmann, 1998). This change in the general pattern indicates reduced tectonic influence.

MFS5, at the transition between the two main patterns, represents a major flooding surface on the platform and is featured worldwide by deposition of "hot shales" during the early Frasnian (Lüning et al., 2004, 2003; Wendt et al., 2006).

The second pattern extends from the "Meden Yahia", "Temertasset" to "Khenig" Formations dated Frasnian to Lower Tournaisian. This pattern is composed of part of D5 to D9 medium-scale sequences. It corresponds to homogenous offshore depositional environments with no lateral facies variations. However, local deltaic (fluvio-marine) conditions are observed during the Frasnian at the Arak Foum Belrem arch (Fig. 10). A successive alternation of shoreface and offshore deposits is organized into five medium-scale sequences (part of D5, and D6 to D9; Figs 9 and 10). This pattern corresponds to the general maximum flooding (Lüning et al., 2003, 2004; Wendt et al., 2006) under eustatic control with no tectonic influences.

6 An association of low rate extensional subsidence and positive inversion pulses

The backstripping approach (Fig. 11) was applied to five wells (W1, W5, W7, W17, and W21). The morphology of the backstripped curve and subsidence rates can provide clues as to the nature of the sedimentary basin (Xie and Heller, 2006). In intracratonic basins, reconstructed tectonic subsidence curves are almost linear to gently exponential in shape, similar to those of passive margins and rifts (Xie and Heller, 2006). The compilation of tectonic backstripped curves from several wells in peri-Hoggar basins (Fig. 11A, see Fig. 1

461 for location) and from wells in the study area (Fig. 11B) display low rates of subsidence (from
462 5 to 50 m/Myr) organized in subsidence patterns of: Inversion of the Low Rate Subsidence
463 (ILRS type c, red line, Fig. 11C), Deceleration of the Low Rate Subsidence (DLRS type b,
464 black line), and Acceleration of the Low Rate Subsidence (ALRS type a, blue line).

465 Each period of ILRS, DLRS, and ALRS may be synchronous among the different wells
466 studied (see B1 to J, Fig. 11B) and some wells of published data (see D to J Fig. 11A).

467 The Saharan Platform is marked by a rejuvenation of basement structures, around arches (Figs
468 2, 3, and 4), linked to regional geodynamic pulses during Neoproterozoic to Paleozoic times
469 (Fig. 11). A compilation of the literature shows that the main geodynamic events are
470 associated with discriminant association of subsidence patterns:

471 (A) Late Pan-African compression and collapse (patterns a, b, and c, A Fig. 11A). The Infra-
472 Cambrian (i.e. top Neoproterozoic) is characterized by horst and graben architecture
473 associated with wedge-shaped unit DO0 in the basement (Fig. 9 and 10). This structuring
474 probably related to Pan-African post-orogenic collapse is illustrated by intracratonic basins
475 infilled with volcano-sedimentary molasses series (Ahmed and Moussine-Pouchkine, 1987;
476 Coward and Ries, 2003; Fabre et al., 1988; Oudra et al., 2005).

477 (B) Cambrian-Ordovician geodynamic pulse (Fig. 11A-B). Highlighted by the wedge-shaped
478 units DO1 (Figs 5A-A' and 6), the horst-graben system is correlated with deceleration (DLRS
479 pattern a, B1) and with local acceleration of the subsidence (ALRS pattern b, B2). The
480 Cambrian–Ordovician extension is documented on arches (Arak-Foum Belrem, Azzel Matti,
481 Amguid El Biod, Tihemboka, Gargaf, Murizidié, Dor El Gussa, etc.) of the Saharan Platform
482 by synsedimentary normal faults, reduced sedimentary successions (Bennacef et al., 1971;
483 Beuf et al., 1971, 1968a, 1968b; Beuf and Montadert, 1962; Borocco and Nyssen, 1959;
484 Claracq et al., 1958; Echikh, 1998; Eschard et al., 2010; Fabre, 1988; Ghienne et al., 2013,

2003; Zazoun and Mahdjoub, 2011) and by stratigraphic hiatuses (Mélou et al., 1999; Oulebsir and Paris, 1995; Paris et al., 2000; Vecoli et al., 1999, 1995).

(C) Late Ordovician geodynamic pulse (i.e. Hirnantian glacial and isostatic rebound; Fig. 11A-B). Late Ordovician incisions mainly situated at the hanging walls of normal faults (Fig. 6C and 6D) are interpreted as Hirnantian glacial valleys (Le Heron, 2010; Smart, 2000) and followed by local inversion of low rate subsidence (ILRS of type c, C in Fig. 11A).

(D) Silurian extensional geodynamic pulse (D, Figs 11A-B). The Silurian post-glaciation period is featured by the reactivation and sealing of the inherited horst and graben fault system (i.e. wedge-shaped unit DO2; Figs 5B-B', 5C-C', 6A and 6B). It is linked to an acceleration of the subsidence (ALRS of pattern b in Fig. 11A-B).

(E) Late Silurian geodynamic pulse (Caledonian compression; E Fig. 11A-B). Late Silurian times are marked by reactivation and local positive inversion of the former structures (Figs 5C-C' and 6B); by truncations located at fold hinges (Figs 5C-C' and 6); and by a major shift from marine to fluvial/transitional environments (Figs 9, 10 supplementary data 2 and 3). Backstripped curves register an inversion of the subsidence (ILRS of pattern c, in Fig. 11A-B). The Caledonian event is mentioned as related to large-scale folding or uplifted arches (e.g. the Gargaff, Tihemboka, Ahara, and Amguid El Biod arches) and it is associated with breaks in the series and with angular unconformities (Beuf et al., 1971; Biju-Duval et al., 1968; Boote et al., 1998; Boudjema, 1987; Boumendjel et al., 1988; Carruba et al., 2014; Chavand and Claracq, 1960; Coward and Ries, 2003; Dubois and Mazelet, 1964; Echikh, 1998; Eschard et al., 2010; Fekirine and Abdallah, 1998; Follot, 1950; Frizon de Lamotte et al., 2013; Ghienne et al., 2013; Gindre et al., 2012; Legrand, 1967b, 1967a; Magloire, 1967).

(F) Early Devonian tectonic quiescence (F Figs 11A-B). This is characterized by a deceleration of the low rate subsidence (DLRS of pattern a, F in Figs 11A-B).

(G) Middle to late Devonian geodynamic pulse (extension and local inversions, G Fig. 11A-B). The Mid to Late Devonian period is characterized by large wedge hiatuses and truncations associated with the reactivation of horst and graben structures and local positive inversion (OD3 in Figs 5D-D', 6, 9, 10 supplementary data 2 and 3). This period is characterized by inversion and acceleration of low rate subsidence (patterns c and b: ILRS - ALRS, Fig. 11A-B). Some of the Middle to Late Devonian hiatuses (Early Eifelian) are noticed in the Ahnet basin (Hassan Kermandji et al., 2008, 2003; Kermandji, 2007; Kermandji et al., 2009; Wendt et al., 2006), in the Reggane (Jäger et al., 2009), on the Amguid Ridge (Wendt et al., 2006), and in the Illizi basin (Boudjema, 1987; Chaumeau et al., 1961).

(H to K) Pre-Hercynian to Hercynian geodynamic pulses (Fig. 11A-B). This period is organized in Early Carboniferous pre-Hercynian (H, Fig. 11A-B) to Late Carboniferous–Early Permian Hercynian (K, Fig. 11A-B) compressions limited by Mid Carboniferous tectonic quiescence (J, Fig. 11A-B). The Carboniferous period is characterized by a normal reactivation and local positive inversion of the previous structural patterns involving reverse faults, overturned folds, transpressional flower structures along strike-slip fault zones (Figs 3, 5F F', 6B, 6C and 6D). The major Carboniferous tectonic event on the Saharan Platform impacted all arches and it is mainly controlled by near-vertical basement faults with a strike-slip component (Boote et al., 1998; Caby, 2003; Liégeois et al., 2003; Haddoum et al., 2001, 2013; Zazoun 2008; J. Wendt et al., 2009 Carruba et al., 2014). Two major hiatuses (i.e. Mid Tournaisian to Mid Visean– Serpukhovian) are recognized (Wendt et al., 2009b).

The geodynamic pulses attest to the reactivation of the terranes and associated lithospheric fault zones. This observation questions the nature of the Precambrian basement and associated structural heritage.

Solid Earth Discuss., https://doi.org/10.5194/se-2018-50
Manuscript under review for journal Solid Earth
Discussion started: 27 June 2018

7 Precambrian structural heritage: accreted lithospheric terranes limited by vertical strike-slip mega shear zones

The 800 km^2 outcrop of basement rocks of the Hoggar shield provides an exceptional case of an exhumed mobile belt composed of accreted terranes of different ages. The Hoggar shield is composed of several accreted, sutured, and amalgamated terranes of various ages and compositions resulting from multiple phases of geodynamic events (Bertrand and Caby, 1978; Black et al., 1994; Caby, 2003; Liégeois et al., 2003).

To reconstruct the nature of the basement, a terrane map (Fig. 12) was put together by integrating geophysical data (aeromagnetic anomaly map: https://www.geomag.us/, Bouguer gravity anomaly map: http://bgi.omp.obs-mip.fr/), satellite images (7ETM+ from Landsat USGS: https://earthexplorer.usgs.gov/) data, geological maps (Berger et al., 2014; Bertrand and Caby, 1978; Black et al., 1994; Caby, 2003; Fezaa et al., 2010; Liégeois et al., 1994, 2003, 2005, 2013), and geochronological data (e.g. U-Pb radiochronology, see supplementary data 5). Geochronological data from published studies were compiled and georeferenced (Fig. 1). Thermo-tectonic ages were grouped into eight main thermo-orogenic events (Archean, Eburnean (i.e. Paleproterozoic), Kibarian (i.e. Mesosproterozoic), Neoproterozoic oceanization-rifting, Neoproterozoic Pan-African orogeny, Caledonian orogeny, and Hercynian orogeny). Geochronological data show that the different terranes were reworked during several main thermo-orogenic events. Twenty-three well preserved terranes in the Hoggar were identified and grouped into Archean, Paleoproterozoic, and Mesoproterozoic–Neoproterozoic juvenile Pan-African terranes (see legend in Fig. 1). In the West African Craton, the Reguibat shield is composed of Archean terrains in the west and of Paleoproterozoic terranes in the east (Peucat et al., 2005, 2003). The two main events deduced from geochronological data are the Neoproterozoic (i.e. Pan-African) and Paleoproterozoic (i.e. Eburnean) episodes (Bertrand and Caby, 1978). Aeromagnetic anomaly surveys are

557 commonly used to analyze geological features such as rock types and fault zones (Gibson and
558 Millegan, 1998; Schubert, 2007; Vacquier et al., 1951). In this study, these data highlight the
559 geometries and the extension of the different terranes under the sedimentary cover. Four main
560 domains can be identified from the aeromagnetic anomaly map, delimited by contrasted
561 magnetic signatures and interpreted as suture zones (thick black lines, Fig. 12A). The study
562 area is bounded to the south by the Tuareg Shield (TS), to the north, by the south Atlasic
563 Range, to the west by the West African Craton (WAC) and at the east by the East Saharan
564 Craton (ESC) or Saharan Metacraton (Abdelsalam et al., 2002).

565 The magnetic disturbance features (Fig. 12A) show three main magnetic trends. A major NS
566 sinuous fabric and two minor sinuous 130–140°E and N45°E trends. The major NS
567 lineaments coincide with terrane boundaries and mega-shear zones (e.g. 4°50', 4°10', WOSZ,
568 EOSZ, 8°30', RSZ shear zones; Fig. 1). Sigmoidal-shaped terranes 200 to 500 km long and
569 100 km wide are characterized (red lines in Fig. 12A). The whole assemblage forms a typical
570 SC-shaped shear fabric (cf. Choukroune et al., 1987) associated with vertical mega-shear
571 zones and suture zones (e.g. WOSZ, EOSZ, 4°10', 4°50' or 8°30' Hoggar shear zones in Fig.
572 1). The SC fabrics combined with subvertical lithospheric shear zones are typical features of
573 the Paleoproterozoic accretionary orogens (Cagnard et al., 2011; Chardon et al., 2009). This
574 architecture is concordant with the Neoproterozoic collage of the Tuareg Shield (i.e. mobile
575 belt) between the West African Craton and the East Saharan Craton (i.e. cratonic blocks)
576 described by Coward and Ries, (2003) and Craig et al. (2006).

577 The gravimetric anomaly map (Fig. 12B) shows a correlation between gravimetric anomalies
578 and tectonic architecture (intracratonic syncline-shaped basin and neighboring arches).
579 Positive anomalies (> 66 mGal) are mainly associated with arches whereas negative
580 anomalies are related to intracratonic basins (< 66 mGal). Nevertheless, negative anomaly
581 disturbance is found in the Hoggar massif probably due to Cenozoic volcanism and the

582 Hoggar swell (Liégeois et al., 2005) or to Eocene Alpine intraplate lithospheric buckling
583 (Rougier et al., 2013). Arches are linked to Archean to Paleoproterozoic continental terranes
584 in contrast to syncline-shaped basins which are associated with Meso-Neoproterozoic terranes
585 (Figs 1 and 12A-B-C).

586 **8 Low subsidence rate intracratonic Paleozoic basins of the Central Sahara provide a**
587 **basis for an integrated modeling study**

588 Paleozoic intracratonic basins with similar characteristics (architecture, subsidence rate,
589 stratigraphic partitioning, alternating episodes of intraplate extension and short duration
590 compressions with periods of tectonic quiescence, etc.) have been documented in North
591 America (e.g. Allen and Armitage, 2011; Beaumont et al., 1988; Burgess, 2008; Burgess et
592 al., 1997; Eaton and Darbyshire, 2010; Pinet et al., 2013; Potter, 2006; Sloss, 1963; Xie and
593 Heller, 2006), South America (e.g. Allen and Armitage, 2011; de Brito Neves et al., 1984; de
594 Oliveira and Mohriak, 2003; Milani and Zalan, 1999; Soares et al., 1978; Zalan et al., 1990),
595 Russia (e.g. Allen and Armitage, 2011; Nikishin et al., 1996) and Australia (e.g. Harris, 1994;
596 Lindsay and Leven, 1996; Mory et al., 2017). However, the nature of the potential driving
597 processes (lithospheric folding, far-field stresses, local increase in the geotherm, mechanical
598 anisotropy from lithospheric rheological heterogeneity, etc.) associated with the formation of
599 intracratonic Paleozoic basins remains highly speculative (e.g. Allen and Armitage, 2011;
600 Armitage and Allen, 2010; Braun et al., 2014; Burgess and Gurnis, 1995; Burov and
601 Cloetingh, 2009; Cacace and Scheck-Wenderoth, 2016; Célérier et al., 2005; Gac et al., 2013;
602 Heine et al., 2008; Leeder, 1991; Vauchez et al., 1998).

603 The multiscale and multidisciplinary analysis performed in this study enable us to document a
604 model of Paleozoic intracratonic Central Saharan basins coupling basin architecture and
605 basement structures (Fig. 13). While we do not provide any quantitative explanations for the
606 dynamics of these basins, our synthesis highlights that their subsidence is not the result of a

single process and we attempt here to make a check-list of the properties that a generic model of formation of such basins must capture:

(A) The association of syncline-shaped wide basins and neighboring arches (i.e. paleo-highs). The structural framework shows a close association of syncline-shaped basins, inter-basin principal to secondary arches, and intra-basin secondary arches (see Fig. 3).

(B) By local horst and graben architecture linked to steep-dipping planar normal faults and associated with normal fault-related fold structures (i.e. forced folds; a, Fig. 13A). Locally, the extensional structures are disrupted by positive inversion structures (b, Fig. 13A) or transported normal faults (c, Fig. 13A).

(C) A low rate of subsidence ranging between 5 to 50 m/Myr (Fig. 11).

(D) Long periods of extension and tectonic quiescence are interrupted by brief periods of compression or glaciation/deglaciation events (Beuf et al., 1971; Denis et al., 2007; Le Heron et al., 2006). These periods of compression are possibly related to intraplate compression linked to distal orogenies (i.e. Late Silurian Caledonian event, Late Carboniferous Hercynian, Frizon de Lamotte et al., 2013, Ziegler et al., 1995) or to intraplate arch uplift related to magmatism (Derder et al., 2016; Fabre, 2005; Frizon de Lamotte et al., 2013; Moreau et al., 1994).

(E) Synsedimentary divergent onlaps and local unconformities are identified from integrated seismic data, satellite images, and borehole data (Figs 4, 5, 6, 9 and 10). The periods of tectonic activity are characterized by normal to reverse reactivation of border faults, emplacement of wedge-shaped units, and erosional unconformities neighboring the arches (Figs 3, 4, 5, 6, 9, 10 and 13).

(F) The stratigraphic architecture displays a lateral facies variation and partitioning between distal marine facies infilling the intracratonic basins (i.e. offshore deposits) and proximal

amalgamated facies (i.e. fluvio-marine, shoreface) associated with prominent stratigraphic hiatus and erosional unconformities in the vicinity of the arches.

(G) A close connection is evidenced between the period of tectonic deformation and the presence of erosional unconformities (i.e. 2, 3, 6, 8, 10 geodynamic events in Fig. 13B). By contrast, the periods of tectonic quiescence and extension are characterized by low lateral facies variations, thin deposits, and the absence of erosional surfaces.

(H) The Precambrian heritage corresponds to Archean to Paleoproterozoic terranes identified in the Hoggar massif and reactivated during the Meso-Neoproterozoic Pan-African cycle (Fig. 1). The Precambrian lithospheric heterogeneity illustrated by the different characteristics of Precambrian terranes (wavelength, age, nature, fault zones) spatially control the emplacement of the syncline-shaped intracratonic basins underlain by Meso–Neoproterozoic oceanic terranes and the arches underlain by Archean to Paleoproterozoic continental terranes (Figs 1, 3 and 13). Many authors suggest control of the basement fabrics is inherited from the Pan-African orogeny in the Saharan basins (Beuf et al., 1968a, 1971; Boote et al., 1998; Carruba et al., 2014; Coward and Ries, 2003; Eschard et al., 2010; Guiraud et al., 2005; Sharata et al., 2015).

9 Conclusion

Our integrated approach using both geophysical (seismic, gravity, aeromagnetic, etc.) and geological (well, seismic, satellite images, etc.) data has enabled us to decrypt the characteristics of the intracratonic Paleozoic Saharan basins and the control of the heterogeneous lithospheric heritage of the horst and graben architecture, low rate subsidence, association of long-lived broad synclines and anticlines (i.e. arches swells, domes, highs or ridges) with very different wavelengths (λ) (tens to hundreds of kilometers). A coupled basin architecture and basement structures model is proposed.

This study highlights a tight control of the heterogeneous lithosphere over the structuring of the intracratonic Central Saharan basin. This particular type of basin is characterized by a low rate of subsidence and fault activation controlling the homogeneity of sedimentary facies and the distribution of the main unconformities. The low rate activation of vertical mega-shear zones bounding the intracratonic basin during Paleozoic times contrasts markedly with classic rift kinematics and architecture. Three different periods of tectonic compressional pulses, extension and quiescence are identified and controlled the sedimentary distribution. An understanding of tectono-sedimentary interaction is key to understanding the distribution of the Paleozoic petroleum reservoirs of this first-order oil province.

Acknowledgements

We are most grateful to ENGIE/NEPTUNE who provided the database used in this paper and who funded the work. Special thanks to the data management service of ENGIE/NEPTUNE (especially Aurelie Galvani) for their help with the database.

References

Abdelsalam, M.G., Liégeois, J.-P., Stern, R.J., 2002. The saharan metacraton. J. Afr. Earth Sci. 34, 119–136.

Abdesselam-Roughi, F., 1977. Etude palynologique du sondage Sebkhet El Melah (No. 022/7.2021). Entreprise nationale Sonatrach division hydrocarbures direction Laboratiore central des hydrocarbures, Boumerdès.

Abdesselam-Rouighi, F., 1991. Résultats de l'étude palynologiques des sondage Garet El Guefoul Bassin de l'Ahnet-Mouydir (No. D000711). Entreprise nationale Sonatrach division hydrocarbures direction Laboratiore central des hydrocarbures, Boumerdès.

Ahmed, A.A.-K., Moussine-Pouchkine, A., 1987. Lithostratigraphie, sédimentologie et évolution de deux bassins molassiques intramontagneux de la chaine Pan-Africaine: la

679 Série pourprée de l'Ahnet, Nord-Ouest du Hoggar, Algérie. J. Afr. Earth Sci. 1983 6,
680 525–535.
681 Aigner, T., 1985. Modern Storm depositional systems: Actualistic models. Springer.
682 Allen, J.R.L., 1983. Studies in fluviatile sedimentation: bars, bar-complexes and sandstone
683 sheets (low-sinuosity braided streams) in the Brownstones (L. Devonian), Welsh
684 Borders. Sediment. Geol. 33, 237–293.
685 Allen, P.A., Allen, J.R., 2005. Basin analysis: Principles and applications, Wiley-Blackwell.
686 ed.
687 Allen, P.A., Armitage, J.J., 2011. Cratonic Basins, in: Busby, C., Azor, A. (Eds.), Tectonics
688 of Sedimentary Basins. John Wiley & Sons, Ltd, pp. 602–620.
689 Angevine, C.L., Heller, P.L., Paola, C., 1990. Quantitative sedimentary basin modeling.
690 American Association of Petroleum Geologists.
691 Armitage, J.J., Allen, P.A., 2010. Cratonic basins and the long-term subsidence history of
692 continental interiors. J. Geol. Soc. 167, 61–70. https://doi.org/10.1144/0016-
693 76492009-108
694 Askri, H., Belmecheri, A., Benrabah, B., Boudjema, A., Boumendjel, K., Daoudi, M., Drid,
695 M., Ghalem, T., Docca, A.M., Ghandriche, H., others, 1995. Geology of Algeria, in:
696 Well Evaluation Conference Algeria. pp. 1–93.
697 Azzoune, N., 1999. Analyse palynologique de trois (03) échantillons de carottes du sondages
698 W7, Sonatrach. Entreprise nationale Sonatrach division hydrocarbures direction
699 Laboratiore central des hydrocarbures, Boumerdès.
700 Badalini, G., Redfern, J., Carr, I.D., 2002. A synthesis of current understanding of the
701 structural evolution of North Africa. J. Pet. Geol. 25, 249–258.
702 Beaumont, C., Quinlan, G., Hamilton, J., 1988. Orogeny and stratigraphy: Numerical models
703 of the Paleozoic in the eastern interior of North America. Tectonics 7, 389–416.

704 Bellahsen, N., Daniel, J.M., 2005. Fault reactivation control on normal fault growth: an
705 experimental study. J. Struct. Geol. 27, 769–780.
706 https://doi.org/10.1016/j.jsg.2004.12.003
707 Bennacef, A., Attar, A., Froukhi, R., Beuf, S., Philippe, G., Schmerber, G., Vermeire, J.C.,
708 1974. Cartes Géologiques d'Iherir-Dider (NG-32-IX), Iherir (NG-32-X), Illizi (NG-
709 32-XV), Aharhar (NG-32-VIII), Oued Samène (NG-32-XIV), Erg Tihodaine (NG-32-
710 VII), Tin Alkoum (NG-32-V), Djanet (NG-32-IV), Ta-N-Mellet (NG-32-XIII) , Ta-N-
711 Elak (NG-32-XIX), Fort Tarat (NG-32-XVI), Tilmas El Mra (NG-31-XXIV), Ers
712 Oum El Lil (NG-31-XXII), Amguid (NG-31-XVIII), 1/200000 Sonatrach-Ministère
713 de l'Industrie et des Mines, Algérie.
714 Bennacef, A., Beuf, S., Biju-Duval, B., Charpal, O. de, Gariel, O., Rognon, P., 1971. Example
715 of Cratonic Sedimentation: Lower Paleozoic of Algerian Sahara. AAPG Bull. 55,
716 2225–2245.
717 Bensalah, A., Beuf, S., Gabriel, O., Philippe, G., Lacot, R., Paris, A., Basseto, D., Conrad, J.,
718 Moussine-Pouchkine, A., 1971. Cartes Géologiques de Khanguet El Hadid (NG-31-
719 XVII), Aïn Tidjoubar (NG-31-XVI), Oued Djaret (NG-31-XV), Aoulef El Arab (NG-
720 31-XIV), Reggane (NG-31-XIII), Ifetessene (NG-31-IX), Arak (NG-31-X et NG-31-
721 IV), Meredoua (NG-31-XIII), Tanezrouft (NG-31-VII et NG-31-I), In Heguis (NG-31-
722 IX), Tin Senasset (NG-31-III), Ouallene (NG-31-II)1/200000 Sonatrach-Ministère de
723 l'Industrie et des Mines, Algérie.
724 Berger, J., Ouzegane, K., Bendaoud, A., Liégeois, J.-P., Kiénast, J.-R., Bruguier, O., Caby,
725 R., 2014. Continental subduction recorded by Neoproterozoic eclogite and garnet
726 amphibolites from Western Hoggar (Tassendjanet terrane, Tuareg Shield, Algeria).
727 Precambrian Res. 247, 139–158. https://doi.org/10.1016/j.precamres.2014.04.002

728 Bertrand, J.M.L., Caby, R., 1978. Geodynamic evolution of the Pan-African orogenic belt: A
729 new interpretation of the Hoggar shield (Algerian Sahara). Geol. Rundsch. 67, 357–
730 388. https://doi.org/10.1007/BF01802795
731 Beuf, S., Biju-Duval, B., De Charpal, O., Gariel, O., 1969. Homogénéité des directions des
732 paléocourants du Dévonien inférieur au Sahara central. Comptes Rendus L'Académie
733 Sci. Sér. D 268, 2026–9.
734 Beuf, S., Biju-Duval, B., De Charpal, O., Gariel, O., Bennacef, A., Black, R., Arene, J.,
735 Boissonnas, J., Chachau, F., Guérangé, B., others, 1968a. Une conséquence directe de
736 la structure du bouclier Africain: L'ébauche des bassins de l'Ahnet et du Mouydir au
737 Paléozoique inférieur. Publ. Serv. Géologique L'Algérie Nouv. Sér. Bull. 38, 105–34.
738 Beuf, S., Biju-Duval, B., de Charpal, O., Rognon, P., Gabriel, O., Bennacef, A., 1971. Les
739 grès du Paléozoïque inférieur au Sahara: Sédimentation et discontinuités évolution
740 structurale d'un craton. Editions TECHNIP.
741 Beuf, S., Biju-Duval, B., Mauvier, A., Legrand, P., 1968b. Nouvelles observations sur le
742 «Cambro-Ordovicien» du Bled el Mass (Sahara central). Paleozoique Inferieur Ahnet
743 Mouydir Rech. Sedimentol. Stratigr. Struct. Algerie Serv Geol Bull 38, 39–52.
744 Beuf, S., Montadert, L., 1962. Sur une discordance angulaire entre les unites II et III du
745 Cambro-Ordovicien au sud-est de la plaine de Dider (Tassili des Ajjers). Compte
746 Rendus Hebd. Séances L'Académie Sci. Paris Ser. Sci. Nat. 254, 1108.
747 Biju-Duval, B., de Charpal, O., Beuf, S., Bennacef, A., 1968. Lithostratigraphie du Dévonien
748 inférieur dans l'Ahnet et le Mouydir (Sahara Central). Bull Serv Géologique Algèrie
749 83–104.
750 Black, R., Latouche, L., Liégeois, J.P., Caby, R., Bertrand, J.M., 1994. Pan-African displaced
751 terranes in the Tuareg shield (central Sahara). Geology 22, 641–644.
752 https://doi.org/10.1130/0091-7613(1994)022<0641:PADTIT>2.3.CO;2

753 Bonini, M., Sani, F., Antonielli, B., 2012. Basin inversion and contractional reactivation of
754 inherited normal faults: A review based on previous and new experimental models.
755 Tectonophysics 522–523, 55–88. https://doi.org/10.1016/j.tecto.2011.11.014
756 Boote, D.R.D., Clark-Lowes, D.D., Traut, M.W., 1998. Palaeozoic petroleum systems of
757 North Africa. Geol. Soc. Lond. Spec. Publ. 132, 7–68.
758 https://doi.org/10.1144/GSL.SP.1998.132.01.02
759 Borocco, J., Nyssen, R., 1959. Nouvelles observations sur les “gres inferieurs” cambro-
760 ordoviciens du Tassili interne (Nord-Hoggar). Bull. Société Géologique Fr. S7–I, 197–
761 206. https://doi.org/10.2113/gssgfbull.S7-I.2.197
762 Boudjema, A., 1987. Evolution structurale du bassin pétrolier “‘triasique’”du Sahara oriental
763 (Algérie). Dr. Diss. Univ Orsay Fr.
764 Boumendjel, K., 1987. Les Chitinozoaires du silurien supérieur et du devonien du Sahara
765 algérien: cadre géologique, systématique, biostratigraphie. ANRT.
766 Boumendjel, K., Loboziak, S., Paris, F., Steemans, P., Streel, M., 1988. Biostratigraphie des
767 Miospores et des Chitinozoaires du Silurien supérieur et du Dévonien dans le bassin
768 d’Illizi (S.E. du Sahara algérien). Geobios 21, 329–357.
769 https://doi.org/10.1016/S0016-6995(88)80057-3
770 Braun, J., Simon-Labric, T., Murray, K.E., Reiners, P.W., 2014. Topographic relief driven by
771 variations in surface rock density. Nat. Geosci. 7, 534–540.
772 https://doi.org/10.1038/ngeo2171
773 Buchanan, P.G., McClay, K.R., 1991. Sandbox experiments of inverted listric and planar fault
774 systems. Tectonophysics 188, 97–115. https://doi.org/10.1016/0040-1951(91)90317-L
775 Burgess, P.M., 2008. Chapter 2 Phanerozoic Evolution of the Sedimentary Cover of the North
776 American Craton, in: Sedimentary Basins of the World. Elsevier, pp. 31–63.
777 https://doi.org/10.1016/S1874-5997(08)00002-6

778 Burgess, P.M., Gurnis, M., 1995. Mechanisms for the formation of cratonic stratigraphic
779 sequences. Earth Planet. Sci. Lett. 136, 647–663. https://doi.org/10.1016/0012-
780 821X(95)00204-P
781 Burgess, P.M., Gurnis, M., Moresi, L., 1997. Formation of sequences in the cratonic interior
782 of North America by interaction between mantle, eustatic, and stratigraphic processes.
783 Geol. Soc. Am. Bull. 109, 1515–1535.
784 Burke, K., MacGregor, D.S., Cameron, N.R., 2003. Africa's petroleum systems: four tectonic
785 "Aces" in the past 600 million years. Geol. Soc. Lond. Spec. Publ. 207, 21–60.
786 Burov, E., Cloetingh, S., 2009. Controls of mantle plumes and lithospheric folding on modes
787 of intraplate continental tectonics: differences and similarities. Geophys. J. Int. 178,
788 1691–1722. https://doi.org/10.1111/j.1365-246X.2009.04238.x
789 Butler, R.W.H., 1989. The influence of pre-existing basin structure on thrust system evolution
790 in the Western Alps. Geol. Soc. Lond. Spec. Publ. 44, 105–122.
791 https://doi.org/10.1144/GSL.SP.1989.044.01.07
792 Caby, R., 2003. Terrane assembly and geodynamic evolution of central–western Hoggar: a
793 synthesis. J. Afr. Earth Sci. 37, 133–159.
794 https://doi.org/10.1016/j.jafrearsci.2003.05.003
795 Cacace, M., Scheck-Wenderoth, M., 2016. Why intracontinental basins subside longer: 3-D
796 feedback effects of lithospheric cooling and sedimentation on the flexural strength of
797 the lithosphere: Subsidence at Intracontinental Basins. J. Geophys. Res. Solid Earth
798 121, 3742–3761. https://doi.org/10.1002/2015JB012682
799 Cagnard, F., Barbey, P., Gapais, D., 2011. Transition between "Archaean-type" and "modern-
800 type" tectonics: Insights from the Finnish Lapland Granulite Belt. Precambrian Res.
801 187, 127–142. https://doi.org/10.1016/j.precamres.2011.02.007

802 Carr, I.D., 2002. Second-Order Sequence Stratigraphy of the Palaeozoic of North Africa. J.
803 Pet. Geol. 25, 259–280. https://doi.org/10.1111/j.1747-5457.2002.tb00009.x
804 Carruba, S., Perotti, C., Rinaldi, M., Bresciani, I., Bertozzi, G., 2014. Intraplate deformation
805 of the Al Qarqaf Arch and the southern sector of the Ghadames Basin (SW Libya). J.
806 Afr. Earth Sci. 97, 19–39. https://doi.org/10.1016/j.jafrearsci.2014.05.001
807 Catuneanu, O., Abreu, V., Bhattacharya, J.P., Blum, M.D., Dalrymple, R.W., Eriksson, P.G.,
808 Fielding, C.R., Fisher, W.L., Galloway, W.E., Gibling, M.R., Giles, K.A., Holbrook,
809 J.M., Jordan, R., Kendall, C.G.S.C., Macurda, B., Martinsen, O.J., Miall, A.D., Neal,
810 J.E., Nummedal, D., Pomar, L., Posamentier, H.W., Pratt, B.R., Sarg, J.F., Shanley,
811 K.W., Steel, R.J., Strasser, A., Tucker, M.E., Winker, C., 2009. Towards the
812 standardization of sequence stratigraphy. Earth-Sci. Rev. 92, 1–33.
813 https://doi.org/10.1016/j.earscirev.2008.10.003
814 Célérier, J., Sandiford, M., Hansen, D.L., Quigley, M., 2005. Modes of active intraplate
815 deformation, Flinders Ranges, Australia. Tectonics 24, n/a-n/a.
816 https://doi.org/10.1029/2004TC001679
817 Chardon, D., Gapais, D., Cagnard, F., 2009. Flow of ultra-hot orogens: A view from the
818 Precambrian, clues for the Phanerozoic. Tectonophysics 477, 105–118.
819 https://doi.org/10.1016/j.tecto.2009.03.008
820 Chaumeau, J., Legrand, P., Renaud, A., 1961. Contribution a l'etude du Couvinien dans le
821 bassin de Fort-de-Polignac (Sahara). Bull. Société Géologique Fr. S7–III, 449–456.
822 https://doi.org/10.2113/gssgfbull.S7-III.5.449
823 Chavand, J.C., Claracq, P., 1960. La disparition du Tassili externe à l'E de Fort-Polignac
824 (Sahara central). CR Soc Géol Fr 1959, 172–174.
825 Choukroune, P., Gapais, D., Merle, O., 1987. Shear criteria and structural symmetry. J. Struct.
826 Geol. 9, 525–530. https://doi.org/10.1016/0191-8141(87)90137-4

827 Claracq, P., Fabre, C., Freulon, J.M., Nougarède, F., 1958. Une discordance angulaire dans
828 les "Grès inférieurs" de l'Adrar Tan Elak (Sahara central)." C. r. Somm. Séances Soc.
829 Géologique Fr. 309–310.
830 Conrad, J., 1984. Les séries carbonifères du Sahara central algérien: stratigraphie,
831 sédimentation, évolution structurale.
832 Conrad, J., 1973. Les grandes lignes stratigraphiques et sédimentologiques du Carbonifere de
833 l'Ahnet-Mouydir (Sahara central algérien). Rev Inst Fr Pet. 28, 3–18.
834 Coward, M.P., Ries, A.C., 2003. Tectonic development of North African basins. Geol. Soc.
835 Lond. Spec. Publ. 207, 61–83. https://doi.org/10.1144/GSL.SP.2003.207.4
836 Cózar, P., Somerville, I.D., Vachard, D., Coronado, I., García-Frank, A., Medina-Varea, P.,
837 Said, I., Del Moral, B., Rodríguez, S., 2016. Upper Mississippian to lower
838 Pennsylvanian biostratigraphic correlation of the Sahara Platform successions on the
839 northern margin of Gondwana (Morocco, Algeria, Libya). Gondwana Res. 36, 459–
840 472. https://doi.org/10.1016/j.gr.2015.07.019
841 Craig, J., Rizzi, C., Thusu, B., Lüning, S., Asbali, A.I., Keeley, M.L., Bell, J.F., Durham,
842 M.J., Eales, M.H., Beswetherick, S., Bishop, C., 2006. Structural Styles and
843 Prospectivity in the Precambrian and Palaeozoic Hydrocarbon Systems of North
844 Africa.
845 Dalrymple, R.W., Choi, K., 2007. Morphologic and facies trends through the fluvial–marine
846 transition in tide-dominated depositional systems: A schematic framework for
847 environmental and sequence-stratigraphic interpretation. Earth-Sci. Rev. 81, 135–174.
848 https://doi.org/10.1016/j.earscirev.2006.10.002
849 Dalrymple, R.W., Mackay, D.A., Ichaso, A.A., Choi, K.S., 2012. Processes,
850 Morphodynamics, and Facies of Tide-Dominated Estuaries, in: Principles of Tidal

Sedimentology. Springer, Dordrecht, pp. 79–107. https://doi.org/10.1007/978-94-007-0123-6_5

Dalrymple, R.W., Zaitlin, B.A., Boyd, R., 1992. A conceptual model of estuarine sedimentation. J. Sediment. Petrol. 62, 116.

de Brito Neves, B.B., Fuck, R.A., Cordani, U.G., Thomaz F°, A., 1984. Influence of basement structures on the evolution of the major sedimentary basins of Brazil: A case of tectonic heritage. J. Geodyn., Precambrian crustal evolution 1, 495–510. https://doi.org/10.1016/0264-3707(84)90021-8

de Oliveira, D.C., Mohriak, W.U., 2003. Jaibaras trough: an important element in the early tectonic evolution of the Parnaíba interior sag basin, Northern Brazil. Mar. Pet. Geol., Paleogeographic reconstruction and hydrocarbon basins: Atlantic, Caribbean, South America, Middle East, Russian Far East, Arctic. 20, 351–383. https://doi.org/10.1016/S0264-8172(03)00044-8

Denis, M., Buoncristiani, J.-F., Konaté, M., Ghienne, J.-F., Guiraud, M., 2007. Hirnantian glacial and deglacial record in SW Djado Basin (NE Niger). Geodin. Acta 20, 177–195. https://doi.org/10.3166/ga.20.177-195

Derder, M.E.M., Maouche, S., Liégeois, J.P., Henry, B., Amenna, M., Ouabadi, A., Bellon, H., Bruguier, O., Bayou, B., Bestandji, R., Nouar, O., Bouabdallah, H., Ayache, M., Beddiaf, M., 2016. Discovery of a Devonian mafic magmatism on the western border of the Murzuq basin (Saharan metacraton): Paleomagnetic dating and geodynamical implications. J. Afr. Earth Sci. 115, 159–176. https://doi.org/10.1016/j.jafrearsci.2015.11.019

Dokka, A.M., 1999. Sedimentological core description WELL: W7, Block - 340, (District - 3), Sonatrach.

875 Dubois, P., 1961. Stratigraphie du Cambro-Ordovicien du Tassili n'Ajjer (Sahara central).
876 Bull. Société Géologique Fr. S7–III, 206–209. https://doi.org/10.2113/gssgfbull.S7-
877 III.2.206
878 Dubois, P., Beuf, S., Biju-Duval, B., 1967. Lithostratigraphie du Dévonien inférieur gréseux
879 du Tassili n 'Ajjer, in: Symposium on the Lower Devonian and Its Limits: Bur.
880 Recherche Geol. et Minieres Mem. pp. 227–235.
881 Dubois, P., Mazelet, P., 1964. Stratigraphie du Silurien du Tassili N'Ajjer. Bull. Société
882 Géologique Fr. S7–VI, 586–591. https://doi.org/10.2113/gssgfbull.S7-VI.4.586
883 Dumas, S., Arnott, R.W.C., 2006. Origin of hummocky and swaley cross-stratification—the
884 controlling influence of unidirectional current strength and aggradation rate. Geology
885 34, 1073–1076.
886 Eaton, D.W., Darbyshire, F., 2010. Lithospheric architecture and tectonic evolution of the
887 Hudson Bay region. Tectonophysics 480, 1–22.
888 https://doi.org/10.1016/j.tecto.2009.09.006
889 Echikh, K., 1998. Geology and hydrocarbon occurrences in the Ghadames basin, Algeria,
890 Tunisia, Libya. Geol. Soc. Lond. Spec. Publ. 132, 109–129.
891 Eschard, R., Abdallah, H., Braik, F., Desaubliaux, G., 2005. The Lower Paleozoic succession
892 in the Tassili outcrops, Algeria: sedimentology and sequence stratigraphy. First Break
893 23.
894 Eschard, R., Braik, F., Bekkouche, D., Rahuma, M.B., Desaubliaux, G., Deschamps, R.,
895 Proust, J.N., 2010. Palaeohighs: their influence on the North African Palaeozoic
896 petroleum systems. Pet. Geol. Mature Basins New Front. 7th Pet. Geol. Conf. 707–
897 724.
898 Eschard, R., Desaubliaux, G., Deschamps, R., Montadert, L., Ravenne, C., Bekkouche, D.,
899 Abdallah, H., Belhaouas, S., Benkouider, M., Braïk, F., Henniche, M., Maache, N.,

Mouaici, R., 1999. Illizi-Berkine Devonian Reservoir Consortium. Institut Française du Pétrole.

Fabre, J., 2005. Géologie du Sahara occidental et central. Musée royal de l'Afrique centrale.

Fabre, J., 1988. Les séries paléozoïques d'Afrique: une approche. J. Afr. Earth Sci. Middle East 7, 1–40. https://doi.org/10.1016/0899-5362(88)90051-6

Fabre, J., Kaci, A.A., Bouima, T., Moussine-Pouchkine, A., 1988. Le cycle molassique dans le Rameau trans-saharien de la chaîne panafricaine. J. Afr. Earth Sci. 7, 41–55. https://doi.org/10.1016/0899-5362(88)90052-8

Fekirine, B., Abdallah, H., 1998. Palaeozoic lithofacies correlatives and sequence stratigraphy of the Saharan Platform, Algeria. Geol. Soc. Lond. Spec. Publ. 132, 97–108. https://doi.org/10.1144/GSL.SP.1998.132.01.05

Fezaa, N., Liégeois, J.-P., Abdallah, N., Cherfouh, E.H., De Waele, B., Bruguier, O., Ouabadi, A., 2010. Late Ediacaran geological evolution (575–555Ma) of the Djanet Terrane, Eastern Hoggar, Algeria, evidence for a Murzukian intracontinental episode. Precambrian Res. 180, 299–327. https://doi.org/10.1016/j.precamres.2010.05.011

Follot, J., 1950. Sur l'existence de mouvements calédoniens au Mouydir (Sahara Central). COMPTES RENDUS Hebd. SEANCES Acad. Sci. 230, 2217–2218.

Frey, R.W., Pemberton, S.G., Saunders, T.D., 1990. Ichnofacies and bathymetry: a passive relationship. J. Paleontol. 64, 155–158.

Frizon de Lamotte, D., Tavakoli-Shirazi, S., Leturmy, P., Averbuch, O., Mouchot, N., Raulin, C., Leparmentier, F., Blanpied, C., Ringenbach, J.-C., 2013. Evidence for Late Devonian vertical movements and extensional deformation in northern Africa and Arabia: Integration in the geodynamics of the Devonian world: Devonian evolution Nothern Gondwana. Tectonics 32, 107–122. https://doi.org/10.1002/tect.20007

924 Fröhlich, S., Petitpierre, L., Redfern, J., Grech, P., Bodin, S., Lang, S., 2010.
925 Sedimentological and sequence stratigraphic analysis of Carboniferous deposits in
926 western Libya: Recording the sedimentary response of the northern Gondwana margin
927 to climate and sea-level changes. J. Afr. Earth Sci. 57, 279–296.
928 https://doi.org/10.1016/j.jafrearsci.2009.09.007
929 Gac, S., Huismans, R.S., Simon, N.S.C., Podladchikov, Y.Y., Faleide, J.I., 2013. Formation
930 of intracratonic basins by lithospheric shortening and phase changes: a case study
931 from the ultra-deep East Barents Sea basin. Terra Nova 25, 459–464.
932 https://doi.org/10.1111/ter.12057
933 Galeazzi, S., Point, O., Haddadi, N., Mather, J., Druesne, D., 2010. Regional geology and
934 petroleum systems of the Illizi–Berkine area of the Algerian Saharan Platform: An
935 overview. Mar. Pet. Geol. 27, 143–178.
936 https://doi.org/10.1016/j.marpetgeo.2008.10.002
937 Galloway, W.E., 1989. Genetic Stratigraphic Sequences in Basin Analysis I: Architecture and
938 Genesis of Flooding-Surface Bounded Depositional Units. ResearchGate 73.
939 https://doi.org/10.1306/703C9AF5-1707-11D7-8645000102C1865D
940 Galushkin, Y.I., Eloghbi, S., 2014. Thermal history of the Murzuq Basin, Libya, and
941 generation of hydrocarbons in its source rocks. Geochem. Int. 52, 486–499.
942 https://doi.org/10.1134/S0016702914060032
943 Gariel, O., de Charpal, O., Bennacef, A., 1968. Sur la sedimentation des gres du Cambro-
944 Ordovicien (Unite II) dans l'Ahnet et le Mouydir (Sahara central): Algerie, Serv.
945 Geol. Bull N Ser 7–37.
946 Ghienne, J.-F., Deynoux, M., Manatschal, G., Rubino, J.-L., 2003. Palaeovalleys and fault-
947 controlled depocentres in the Late-Ordovician glacial record of the Murzuq Basin

(central Libya). Comptes Rendus Geosci. 335, 1091–1100. https://doi.org/10.1016/j.crte.2003.09.010

Ghienne, J.-F., Moreau, J., Degermann, L., Rubino, J.-L., 2013. Lower Palaeozoic unconformities in an intracratonic platform setting: glacial erosion versus tectonics in the eastern Murzuq Basin (southern Libya). Int. J. Earth Sci. 102, 455–482. https://doi.org/10.1007/s00531-012-0815-y

Gibson, R.I., Millegan, P.S. (Eds.), 1998. Geologic applications of gravity and magnetics: case histories, AAPG studies in geology. Published jointly by the Society of Exploration Geophysicists and the American Association of Petroleum Geologists, Tulsa, OK.

Gindre, L., Le Heron, D., Bjørnseth, H.M., 2012. High resolution facies analysis and sequence stratigraphy of the Siluro-Devonian succession of Al Kufrah basin (SE Libya). J. Afr. Earth Sci. 76, 8–26. https://doi.org/10.1016/j.jafrearsci.2012.08.002

Grasemann, B., Martel, S., Passchier, C., 2005. Reverse and normal drag along a fault. J. Struct. Geol. 27, 999–1010. https://doi.org/10.1016/j.jsg.2005.04.006

Greigertt, J., Pougnet, R., 1965. Carte Géologique du Niger, 1/2000000, BRGM, Répulbique du Niger.

Guiraud, R., Bosworth, W., Thierry, J., Delplanque, A., 2005. Phanerozoic geological evolution of Northern and Central Africa: An overview. J. Afr. Earth Sci. 43, 83–143. https://doi.org/10.1016/j.jafrearsci.2005.07.017

Haddoum, H., Mokri, M., Ouzegane, K., Ait-Djaffer, S., Djemai, S., 2013. Extrusion de l'In Ouzzal vers le Nord (Hoggar occidental, Algérie): une conséquence d'un poinçonnement panafricain. J. Hydrocarb. Mines Environ. Res. Vol. 4, 6–16.

Haq, B.U., Schutter, S.R., 2008. A Chronology of Paleozoic Sea-Level Changes. Science 322, 64–68. https://doi.org/10.1126/science.1161648

973 Harris, L.B., 1994. Structural and tectonic synthesis for the Perth basin, Western Australia. J.
974 Pet. Geol. 17, 129–156.
975 Hartley, R.W., Allen, P.A., 1994. Interior cratonic basins of Africa: relation to continental
976 break-up and role of mantle convection. Basin Res. 6, 95–113.
977 Hassan, A., 1984. Etude palynologique Paléozoïque du sondage Razzal-Allah-Nord (No.
978 501/1.2018). Entreprise nationale Sonatrach division hydrocarbures direction
979 Laboratiore central des hydrocarbures, Boumerdès.
980 Hassan Kermandji, A.M., Kowalski, M.W., Pharisat, A., 2003. Palynologie et séquences de
981 l'Emsien de la région d'In Salah, Sahara central Algérien. Bull. Société D'Histoire
982 Nat. Pays Montbél. 301–306.
983 Hassan Kermandji, A.M., Kowalski, W.M., Touhami, F.K., 2008. Miospore stratigraphy of
984 Lower and early Middle Devonian deposits from Tidikelt, Central Sahara, Algeria.
985 Geobios 41, 227–251. https://doi.org/10.1016/j.geobios.2007.05.002
986 Heine, C., Dietmar Müller, R., Steinberger, B., Torsvik, T.H., 2008. Subsidence in
987 intracontinental basins due to dynamic topography. Phys. Earth Planet. Inter. 171,
988 252–264. https://doi.org/10.1016/j.pepi.2008.05.008
989 Henniche, M., 2002. Architecture et modèle de dépôts d'une série sédimentaire paléozoïque
990 en contexte cratonique. Rennes 1.
991 Holbrook, J., Schumm, S.A., 1999. Geomorphic and sedimentary response of rivers to
992 tectonic deformation: a brief review and critique of a tool for recognizing subtle
993 epeirogenic deformation in modern and ancient settings. Tectonophysics 305, 287–
994 306.
995 Hollard, H., Choubert, G., Bronner, G., Marchand, J., Sougy, J., 1985. Carte géologique du
996 Maroc, scale 1: 1,000,000. Serv Carte Géol Maroc 260.

997 Holt, P.J., Allen, M.B., van Hunen, J., Bjørnseth, H.M., 2010. Lithospheric cooling and
998 thickening as a basin forming mechanism. Tectonophysics 495, 184–194.
999 https://doi.org/10.1016/j.tecto.2010.09.014
1000 Jacquemont, P., Jutard, G., Plauchut, B., Grégoire, J., Mouflard, R., 1959. Etude du bassin du
1001 Djado. Bur. Rech. Pétroles Rapp. 1215.
1002 Jäger, H., Lewandowski, E., Lampart, V., 2009. Palynology of the upper Silurian to middle
1003 Devonian in the Reggane Basin, southern Algeria.
1004 Jardiné, S., Yapaudjian, L., 1968. Lithostratigraphie et palynologie du Dévonien-Gothlandien
1005 gréseux du Bassin de Polignac (Sahara). Rev. L'Institut Fr. Pétrole 23, 439–469.
1006 Joulia, F., 1963. Carte géologique de reconnaissance de la bordure sédimentaire occidentale
1007 de l'Aïr au 1/500 000. Éditions BRGM Orléans Fr.
1008 Kermandji, A.M.H., 2007. Silurian–Devonian miospores from the western and central
1009 Algeria. Rev. Micropaléontologie 50, 109–128.
1010 https://doi.org/10.1016/j.revmic.2007.01.003
1011 Kermandji, A.M.H., Touhami, F.K., Kowalski, W.M., Abbés, S.B., Boularak, M., Chabour,
1012 N., Laifa, E.L., Hannachi, H.B., 2009. Stratigraphie du Dévonien Inférieur du Plateau
1013 du Tidikelt d'In Salah (Sahara Central Algérie). Comun. Geológicas 67–82.
1014 Khalil, S.M., McClay, K.R., 2002. Extensional fault-related folding, northwestern Red Sea,
1015 Egypt. J. Struct. Geol. 24, 743–762.
1016 Khiar, S., 1974. Résultats palynologiques du sondage Garet El Guefoul (No. D000714).
1017 Entreprise nationale Sonatrach division hydrocarbures direction Laboratiore central
1018 des hydrocarbures, Alger.
1019 Le Heron, D.P., 2010. Interpretation of Late Ordovician glaciogenic reservoirs from 3-D
1020 seismic data: an example from the Murzuq Basin, Libya. Geol. Mag. 147, 28.
1021 https://doi.org/10.1017/S0016756809990586

Le Heron, D.P., Craig, J., Etienne, J.L., 2009. Ancient glaciations and hydrocarbon accumulations in North Africa and the Middle East. Earth-Sci. Rev. 93, 47–76. https://doi.org/10.1016/j.earscirev.2009.02.001

Le Heron, D.P., Craig, J., Sutcliffe, O.E., Whittington, R., 2006. Late Ordovician glaciogenic reservoir heterogeneity: An example from the Murzuq Basin, Libya. Mar. Pet. Geol. 23, 655–677. https://doi.org/10.1016/j.marpetgeo.2006.05.006

Leeder, M.R., 1991. Denudation, vertical crustal movements and sedimentary basin infill. Geol. Rundsch. 80, 441–458. https://doi.org/10.1007/BF01829376

Legrand, P., 2003. Late Ordovician-early Silurian paleogeography of the Algerian Sahara. Bull. Société Géologique Fr. 174, 19–32.

Legrand, P., 1996. Silurian stratigraphy and paleogeography of the northern African margin of Gondwana, in: 2nd Int. Symp. Silurian System.

Legrand, P., 1986. The lower Silurian graptolites of Oued In Djerane: a study of populations at the Ordovician-Silurian boundary. Geol. Soc. Lond. Spec. Publ. 20, 145–153. https://doi.org/10.1144/GSL.SP.1986.020.01.15

Legrand, P., 1967a. Le Devonien du Sahara Algerien 245–284.

Legrand, P., 1967b. Nouvelles connaissances acquises sur la limite des systèmes Silurien et Dévonien au Sahara algérien. Bull. Bur. Rech. Géologiques Minières 33, 119–37.

Legrand-Blain, M., 1985. Dynamique des Brachiopodes carbonifères sur la plate-forme carbonatée du Sahara algérien: paléoenvironnements, paléobiogéographie, évolution.

Lessa, G., Masselink, G., 1995. Morphodynamic evolution of a macrotidal barrier estuary. Mar. Geol. 129, 25–46.

Leuven, J.R.F.W., Kleinhans, M.G., Weisscher, S.A.H., van der Vegt, M., 2016. Tidal sand bar dimensions and shapes in estuaries. Earth-Sci. Rev. 161, 204–223. https://doi.org/10.1016/j.earscirev.2016.08.004

1047 Lewis, M.M., Jackson, C.A.-L., Gawthorpe, R.L., Whipp, P.S., 2015. Early synrift reservoir
1048 development on the flanks of extensional forced folds: A seismic-scale outcrop analog
1049 from the Hadahid fault system, Suez rift, Egypt. AAPG Bull. 99, 985–1012.
1050 https://doi.org/10.1306/12011414036
1051 Liégeois, J.-P., Abdelsalam, M.G., Ennih, N., Ouabadi, A., 2013. Metacraton: Nature, genesis
1052 and behavior. Gondwana Res. 23, 220–237. https://doi.org/10.1016/j.gr.2012.02.016
1053 Liégeois, J.-P., Benhallou, A., Azzouni-Sekkal, A., Yahiaoui, R., Bonin, B., 2005. The
1054 Hoggar swell and volcanism: Reactivation of the Precambrian Tuareg shield during
1055 Alpine convergence and West African Cenozoic volcanism. Geol. Soc. Am. Spec.
1056 Pap. 388, 379–400. https://doi.org/10.1130/0-8137-2388-4.379
1057 Liégeois, J.-P., Black, R., Navez, J., Latouche, L., 1994. Early and late Pan-African orogenies
1058 in the Air assembly of terranes (Tuareg Shield, Niger). Precambrian Res. 67, 59–88.
1059 Liégeois, J.P., Latouche, L., Boughrara, M., Navez, J., Guiraud, M., 2003. The LATEA
1060 metacraton (Central Hoggar, Tuareg shield, Algeria): behaviour of an old passive
1061 margin during the Pan-African orogeny. J. Afr. Earth Sci. 37, 161–190.
1062 https://doi.org/10.1016/j.jafrearsci.2003.05.004
1063 Lindsay, J.F., Leven, J.H., 1996. Evolution of a Neoproterozoic to Palaeozoic intracratonic
1064 setting, Officer Basin, South Australia. Basin Res. 8, 403–424.
1065 https://doi.org/10.1046/j.1365-2117.1996.00223.x
1066 Logan, P., Duddy, I., 1998. An investigation of the thermal history of the Ahnet and Reggane
1067 Basins, Central Algeria, and the consequences for hydrocarbon generation and
1068 accumulation. Geol. Soc. Lond. Spec. Publ. 132, 131–155.
1069 Loi, A., Ghienne, J.-F., Dabard, M.P., Paris, F., Botquelen, A., Christ, N., Elaouad-Debbaj,
1070 Z., Gorini, A., Vidal, M., Videt, B., Destombes, J., 2010. The Late Ordovician glacio-
1071 eustatic record from a high-latitude storm-dominated shelf succession: The Bou Ingarf

section (Anti-Atlas, Southern Morocco). Palaeogeogr. Palaeoclimatol. Palaeoecol. 296, 332–358. https://doi.org/10.1016/j.palaeo.2010.01.018

Lubeseder, S., 2005. Silurian and Devonian sequence stratigraphy of North Africa; Regional correlation and sedimentology (Marocco, Algeria, Libya). University of Manchester.

Lubeseder, S., Redfern, J., Petitpierre, L., Fröhlich, S., 2010. Stratigraphic trapping potential in the Carboniferous of North Africa: developing new play concepts based on integrated outcrop sedimentology and regional sequence stratigraphy (Morocco, Algeria, Libya), in: Petroleum Geology: From Mature Basins to New Frontiers—Proceedings of the 7th Petroleum Geology Conference. Geological Society of London, pp. 725–734.

Lüning, S., 2005. North African Phanerozoic.

Lüning, S., Adamson, K., Craig, J., 2003. Frasnian organic-rich shales in North Africa: regional distribution and depositional model. Geol. Soc. Lond. Spec. Publ. 207, 165–184. https://doi.org/10.1144/GSL.SP.2003.207.9

Lüning, S., Craig, J., Loydell, D.K., Štorch, P., Fitches, B., 2000. Lower Silurian `hot shales' in North Africa and Arabia: regional distribution and depositional model. Earth-Sci. Rev. 49, 121–200. https://doi.org/10.1016/S0012-8252(99)00060-4

Lüning, S., Wendt, J., Belka, Z., Kaufmann, B., 2004. Temporal–spatial reconstruction of the early Frasnian (Late Devonian) anoxia in NW Africa: new field data from the Ahnet Basin (Algeria). Sediment. Geol. 163, 237–264. https://doi.org/10.1016/S0037-0738(03)00210-0

Madritsch, H., Schmid, S.M., Fabbri, O., 2008. Interactions between thin- and thick-skinned tectonics at the northwestern front of the Jura fold-and-thrust belt (eastern France): THIN AND THICK TECTONICS AT JURA FRONT. Tectonics 27, n/a-n/a. https://doi.org/10.1029/2008TC002282

1097 Magloire, L., 1967. Étude stratigraphique, par la Palynologie, des dépôts argilo-gréseux du
1098 Silurien et du Dévonien inférieur dans la Région du Grand Erg Occidental (Sahara
1099 Algérien).
1100 Makhous, M., Galushkin, Y.I., 2003a. Burial history and thermal evolution of the southern
1101 and western Saharan basins: Synthesis and comparison with the eastern and northern
1102 Saharan basins. AAPG Bull. 87, 1799–1822.
1103 Makhous, M., Galushkin, Y.I., 2003b. Burial history and thermal evolution of the northern
1104 and eastern Saharan basins. AAPG Bull. 87, 1623–1651.
1105 https://doi.org/10.1306/04300301122
1106 Marchal, D., Guiraud, M., Rives, T., 2003. Geometric and morphologic evolution of normal
1107 fault planes and traces from 2D to 4D data. J. Struct. Geol. 25, 135–158.
1108 https://doi.org/10.1016/S0191-8141(02)00011-1
1109 Marchal, D., Guiraud, M., Rives, T., van den Driessche, J., 1998. Space and time propagation
1110 processes of normal faults. Geol. Soc. Lond. Spec. Publ. 147, 51–70.
1111 https://doi.org/10.1144/GSL.SP.1998.147.01.04
1112 Massa, D., 1988. Paléozoïque de Libye occidentale : stratigraphie et paléogéographie. Nice.
1113 Mélou, M., Oulebsir, L., Paris, F., 1999. Brachiopodes et chitinozoaires ordoviciens dans le
1114 NE du Sahara algérien: Implications stratigraphiques et paléogéographiques. Geobios
1115 32, 822–839. https://doi.org/10.1016/S0016-6995(99)80865-1
1116 Milani, E.J., Zalan, P.V., 1999. An outline of the geology and petroleum systems of the
1117 Paleozoic interior basins of South America. Episodes 22, 199–205.
1118 Milton, N.J., Bertram, G.T., Vann, I.R., 1990. Early Palaeogene tectonics and sedimentation
1119 in the Central North Sea. Geol. Soc. Lond. Spec. Publ. 55, 339–351.

Moreau, C., Demaiffe, D., Bellion, Y., Boullier, A.-M., 1994. A tectonic model for the location of Palaeozoic ring complexes in Air (Niger, West Africa). Tectonophysics 234, 129–146.

Mory, A.J., Zhan, Y., Haines, P.W., Hocking, R.M., Thomas, C.M., Copp, I.A., 2017. A paleozoic perspective of Western Australia.

Nikishin, A.M., Ziegler, P.A., Stephenson, R.A., Cloetingh, S., Furne, A.V., Fokin, P.A., Ershov, A.V., Bolotov, S.N., Korotaev, M.V., Alekseev, A.S., 1996. Late Precambrian to Triassic history of the East European Craton: dynamics of sedimentary basin evolution. Tectonophysics 268, 23–63.

Ogg, J.G., Ogg, G., Gradstein, F.M., 2016. A Concise Geologic Time Scale: 2016. Elsevier.

Oudra, M., Beraaouz, H., Ikenne, M., Gasquet, D., Soulaimani, A., 2005. La Tectonique Panafricaine du Secteur d'Igherm: Implication des dômes extensifs tardi à post-orogéniques (Anti-Atlas occidental, Maroc). Estud. Geológicos 61, 177–189.

Oulebsir, L., Paris, F., 1995. Chitinozoaires ordoviciens du Sahara algérien: biostratigraphie et affinités paléogéographiques. Rev. Palaeobot. Palynol. 86, 49–68. https://doi.org/10.1016/0034-6667(94)00098-5

Owen, G., 1995. Senni Beds of the Devonian Old Red Sandstone, Dyfed, Wales: anatomy of a semi-arid floodplain. Sediment. Geol. 95, 221–235.

Paris, F., 1990. The Ordovician chitinozoan biozones of the Northern Gondwana domain. Rev. Palaeobot. Palynol. 66, 181–209. https://doi.org/10.1016/0034-6667(90)90038-K

Paris, F., Bourahrouh, A., Hérissé, A.L., 2000. The effects of the final stages of the Late Ordovician glaciation on marine palynomorphs (chitinozoans, acritarchs, leiospheres) in well Nl-2 (NE Algerian Sahara). Rev. Palaeobot. Palynol. 113, 87–104. https://doi.org/10.1016/S0034-6667(00)00054-3

1144 Pemberton, S.G., Frey, R.W., 1982. Trace fossil nomenclature and the Planolites-
1145 Palaeophycus dilemma. J. Paleontol. 843–881.
1146 Peucat, J.-J., Capdevila, R., Drareni, A., Mahdjoub, Y., Kahoui, M., 2005. The Eglab massif
1147 in the West African Craton (Algeria), an original segment of the Eburnean orogenic
1148 belt: petrology, geochemistry and geochronology. Precambrian Res. 136, 309–352.
1149 https://doi.org/10.1016/j.precamres.2004.12.002
1150 Peucat, J.J., Drareni, A., Latouche, L., Deloule, E., Vidal, P., 2003. U–Pb zircon (TIMS and
1151 SIMS) and Sm–Nd whole-rock geochronology of the Gour Oumelalen granulitic
1152 basement, Hoggar massif, Tuareg shield, Algeria. J. Afr. Earth Sci. 37, 229–239.
1153 https://doi.org/10.1016/j.jafrearsci.2003.03.001
1154 Pinet, N., Lavoie, D., Dietrich, J., Hu, K., Keating, P., 2013. Architecture and subsidence
1155 history of the intracratonic Hudson Bay Basin, northern Canada. Earth-Sci. Rev. 125,
1156 1–23. https://doi.org/10.1016/j.earscirev.2013.05.010
1157 Potter, D., 2006. Relationships of Cambro-Ordovician stratigraphy to paleotopography on the
1158 Precambrian basement, Williston Basin.
1159 Reading, H.G. (Ed.), 2002. Sedimentary environments: processes, facies, and stratigraphy,
1160 3rd ed. ed. Blackwell Science, Oxford ; Cambridge, Mass.
1161 Rider, M.H., 1996. The geological interpretation of well logs, 2nd ed. ed. Caithness,
1162 Scotland : Whittles.
1163 Rougier, S., Missenard, Y., Gautheron, C., Barbarand, J., Zeyen, H., Pinna, R., Liégeois, J.-P.,
1164 Bonin, B., Ouabadi, A., Derder, M.E.-M., Lamotte, D.F. de, 2013. Eocene exhumation
1165 of the Tuareg Shield (Sahara Desert, Africa). Geology 41, 615–618.
1166 https://doi.org/10.1130/G33731.1
1167 Schlische, R.W., 1995. Geometry and origin of fault-related folds in extensional settings.
1168 AAPG Bull. 79, 1661–1678.

1169 Schubert, G., 2007. Treatise on Geophysics. Blackwell Pub, Malden, MA.
1170 Sclater, J.G., Christie, P.A.F., 1980. Continental stretching: An explanation of the Post-Mid-
1171 Cretaceous subsidence of the central North Sea Basin. J. Geophys. Res. Solid Earth
1172 85, 3711–3739. https://doi.org/10.1029/JB085iB07p03711
1173 Scotese, C.R., Boucot, A.J., McKerrow, W.S., 1999. Gondwanan palaeogeography and
1174 paleoclimatology. J. Afr. Earth Sci. 28, 99–114. https://doi.org/10.1016/S0899-
1175 5362(98)00084-0
1176 Serra, O., 2009. Well logging and geology. Technip Editions.
1177 Sharata, S., Röth, J., Reicherter, K., 2015. Basin evolution in the North African Platform.
1178 Geotecton. Res. 97, 80–81. https://doi.org/10.1127/1864-5658/2015-31
1179 Shaw, J.H., Connors, C.D., Suppe, J., 2005. Seismic interpretation of contractional fault-
1180 related folds: an AAPG seismic atlas. American Association of Petroleum Geologists,
1181 Tulsa, Okla., U.S.A.
1182 Sloss, L.L., 1963. Sequences in the cratonic interior of North America. Geol. Soc. Am. Bull.
1183 74, 93–114.
1184 Smart, J., 2000. Seismic expressions of depositional processes in the upper Ordovician
1185 succession of the Murzuq Basin, SW Libya-Chapter 19.
1186 Soares, P.C., LANDIM, P.M.B., Fulfaro, V.J., 1978. Tectonic cycles and sedimentary
1187 sequences in the Brazilian intracratonic basins. Geol. Soc. Am. Bull. 89, 181–191.
1188 Stow, D. a. V., Piper, D.J.W., 1984. Deep-water fine-grained sediments: facies models. Geol.
1189 Soc. Lond. Spec. Publ. 15, 611–646. https://doi.org/10.1144/GSL.SP.1984.015.01.38
1190 Stow, D.A.V., Huc, A.-Y., Bertrand, P., 2001. Depositional processes of black shales in deep
1191 water. Mar. Pet. Geol. 18, 491–498. https://doi.org/10.1016/S0264-8172(01)00012-5
1192 Suter, J.R., 2006. Facies models revisited: clastic shelves. Spec. Publ.-SEPM 84, 339.

Tournier, F., 2010. Mécanismes et contrôle des phénomènes diagénétiques en milieu acide dans les grès de l'Ordovicien glaciaire du bassin de Sbaa, Algérie. Université de Paris-Sud. Faculté des Sciences d'Orsay (Essonne).

Trompette, R., 2000. Gondwana evolution; its assembly at around 600 Ma. Comptes Rendus Académie Sci.-Ser. IIA-Earth Planet. Sci. 330, 305–315.

Ustaszewski, K., Schumacher, M., Schmid, S., Nieuwland, D., 2005. Fault reactivation in brittle?viscous wrench systems?dynamically scaled analogue models and application to the Rhine?Bresse transfer zone. Quat. Sci. Rev. 24, 363–380. https://doi.org/10.1016/j.quascirev.2004.03.015

Vacquier, V., Steenland, N.C., Henderson, R.G., Zietz, I., 1951. Interpretation of aeromagnetic maps. Geol. Soc. Am. Mem. 47, 1–150.

Van Hinte, J.E., 1978. Geohistory analysis–application of micropaleontology in exploration geology. AAPG Bull. 62, 201–222.

Vauchez, A., Tommasi, A., Barruol, G., 1998. Rheological heterogeneity, mechanical anisotropy and deformation of the continental lithosphere. Tectonophysics 296, 61–86. https://doi.org/10.1016/S0040-1951(98)00137-1

Vecoli, M., Albani, R., Ghomari, A., Massa, D., Tongiorgi, M., 1995. Précisions sur la limite Cambrien-Ordovicien au Sahara Algérien (Secteur de Hassi-Rmel). Comptes Rendus Académie Sci. Sér. 2 Sci. Terre Planètes 320, 515–522.

Vecoli, M., Tongiorgi, M., Abdesselam-Roughi, F.F., Benzarti, R., Massa, D., 1999. Palynostratigraphy of upper Cambrian-upper Ordovician intracratonic clastic sequences, North Africa. Boll.-Soc. Paleontol. Ital. 38, 331–342.

Videt, B., Paris, F., Rubino, J.-L., Boumendjel, K., Dabard, M.-P., Loi, A., Ghienne, J.-F., Marante, A., Gorini, A., 2010. Biostratigraphical calibration of third order Ordovician

sequences on the northern Gondwana platform. Palaeogeogr. Palaeoclimatol. Palaeoecol. 296, 359–375. https://doi.org/10.1016/j.palaeo.2010.03.050

Wagoner, J.C.V., Mitchum, R.M., Campion, K.M., Rahmanian, V.D., 1990. Siliciclastic Sequence Stratigraphy in Well Logs, Cores, and Outcrops: Concepts for High-Resolution Correlation of Time and Facies 174, III-55.

Watts, A.B., 2001. Isostasy and Flexure of the Lithosphere. Cambridge University Press.

Wendt, J., 1995. Shell directions as a tool in palaeocurrent analysis. Sediment. Geol. 95, 161–186. https://doi.org/10.1016/0037-0738(94)00104-3

Wendt, J., 1988. Facies Pattern and Paleogeography of the Middle and Late Devonian in the Eastern Anti-Atlas (Morocco) 467–480.

Wendt, J., 1985. Disintegration of the continental margin of northwestern Gondwana: Late Devonian of the eastern Anti-Atlas (Morocco). Geology 13, 815–818.

Wendt, J., Belka, Z., Kaufmann, B., Kostrewa, R., Hayer, J., 1997. The world's most spectacular carbonate mud mounds (Middle Devonian, Algerian Sahara). J. Sediment. Res. 67, 424–436. https://doi.org/10.1306/D426858B-2B26-11D7-8648000102C1865D

Wendt, J., Belka, Z., Moussine-Pouchkine, A., 1993. New architectures of deep-water carbonate buildups: Evolution of mud mounds into mud ridges (Middle Devonian, Algerian Sahara). Geology 21, 723–726.

Wendt, J., Kaufmann, B., 1998. Mud buildups on a Middle Devonian carbonate ramp (Algerian Sahara). Geol. Soc. Lond. Spec. Publ. 149, 397–415. https://doi.org/10.1144/GSL.SP.1999.149.01.18

Wendt, J., Kaufmann, B., Belka, Z., 2009a. Devonian stratigraphy and depositional environments in the southern Illizi Basin (Algerian Sahara). J. Afr. Earth Sci. 54, 85–96. https://doi.org/10.1016/j.jafrearsci.2009.03.006

Wendt, J., Kaufmann, B., Belka, Z., Klug, C., Lubeseder, S., 2006. Sedimentary evolution of a Palaeozoic basin and ridge system: the Middle and Upper Devonian of the Ahnet and Mouydir (Algerian Sahara). Geol. Mag. 143, 269. https://doi.org/10.1017/S0016756806001737

Wendt, J., Kaufmann, B., Belka, Z., Korn, D., 2009b. Carboniferous stratigraphy and depositional environments in the Ahnet Mouydir area (Algerian Sahara). Facies 55, 443–472. https://doi.org/10.1007/s10347-008-0176-y

Withjack, M.O., Callaway, S., 2000. Active normal faulting beneath a salt layer: an experimental study of deformation patterns in the cover sequence. AAPG Bull. 84, 627–651.

Withjack, M.O., Olson, J., Peterson, E., 1990. Experimental models of extensional forced folds (1). Aapg Bull. 74, 1038–1054.

Withjack, M.O., Schlische, R.W., Olsen, P.E., 2002. Rift-basin structure and its influence on sedimentary systems.

Xie, X., Heller, P., 2006. Plate tectonics and basin subsidence history. Geol. Soc. Am. Bull. preprint, 1. https://doi.org/10.1130/B26398.1

Yahi, N., 1999. Petroleum generation and migration in the Berkine (Ghadames) Basin, Eastern Algeria: an organic geochemical and basin modelling study. Forschungszentrum, Zentralbibliothek, Jülich.

Zalan, P.V., Wolff, S., Astolfi, M.A.M., Vieira, I.S., Concelcao, J.C.J., Appi, V.T., Neto, E.V.S., Cerqueira, J.R., Marques, A., 1990. The Parana Basin, Brazil: Chapter 33: Part II. Selected Analog Interior Cratonic Basins: Analog Basins 134, 681–708.

Zazoun, R.S., Mahdjoub, Y., 2011. Strain analysis of Late Ordovician tectonic events in the In-Tahouite and Tamadjert Formations (Tassili-n-Ajjers area, Algeria). J. Afr. Earth Sci. 60, 63–78. https://doi.org/10.1016/j.jafrearsci.2011.02.003

Solid Earth Discuss., https://doi.org/10.5194/se-2018-50
Manuscript under review for journal Solid Earth
Discussion started: 27 June 2018

1269 **List of figures**

Solid Earth Discuss., https://doi.org/10.5194/se-2018-50
Manuscript under review for journal Solid Earth
Discussion started: 27 June 2018

Solid Earth
Discussions
Open Access
EGU

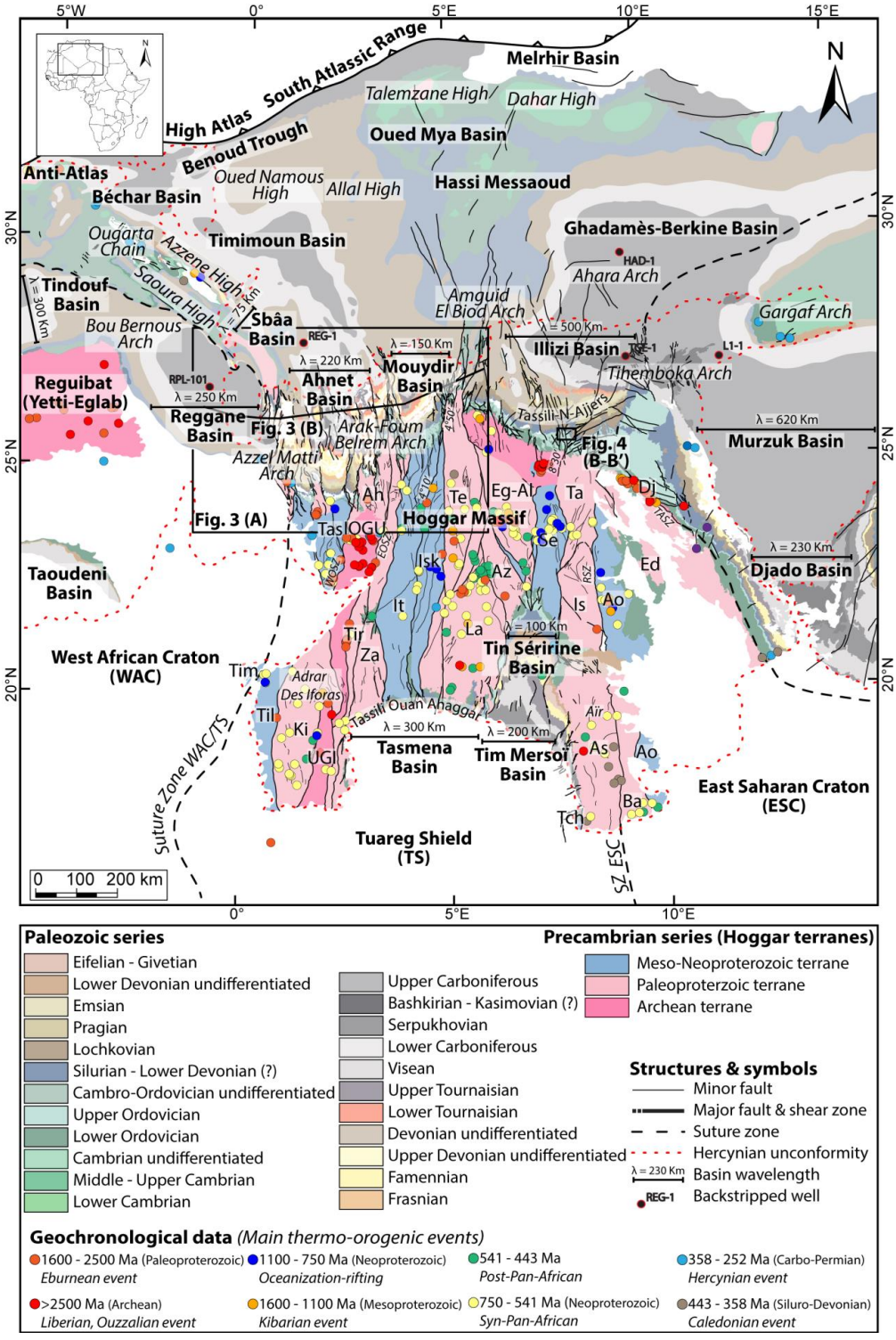

Solid Earth Discuss., https://doi.org/10.5194/se-2018-50
Manuscript under review for journal Solid Earth
Discussion started: 27 June 2018

Figure 1: Geological map of the Paleozoic North Saharan Platform (North Gondwana) georeferenced, compiled and modified from (1) Paleozoic subcrop distribution below the Hercynian unconformity geology of the Saharan Platform (Boote et al., 1998; Galeazzi et al., 2010); (2) Geological map (1/500000) of the Djado basin (Jacquemont et al., 1959); (3) Geological map (1/20000) of Algeria (Bennacef et al., 1974; Bensalah et al., 1971), (4) Geological map (1/50000) of Aïr (Joulia, 1963), (5) Geological map (1/2000000) of Niger (Greigertt and Pougnet, 1965), (6) Geological map (1/5000000) of the Lower Paleozoic of the Central Sahara (Beuf et al., 1971), (7) Geological map (1/1000000) of Morocco (Hollard et al., 1985), (8) Geological map of the Djebel Fezzan (Massa, 1988); Basement characterization of the different terranes from geochronological data compilation (see supplementary data) and geological maps (Berger et al., 2014; Bertrand and Caby, 1978; Black et al., 1994; Caby, 2003; Fezaa et al., 2010; Liégeois et al., 1994, 2003, 2005, 2013); Terrane names: Tassendjanet (Tas), Tassendjanet nappe (Tas n.), Ahnet (Ah), In Ouzzal Granulitic Unit (IOGU), Iforas Granulitic Unit (UGI), Kidal (Ki), Timétrine (Tim), Tilemsi (Til), Tirek (Tir), In Zaouatene (Za), In Teidini (It), Iskel (Isk), Tefedest (Te), Laouni (La), Azrou-n-Fad (Az), Egéré-Aleskod (Eg-Al), Serouenout (Se), Tazat (Ta), Issalane (Is), Assodé (As), Barghot (Ba), Tchilit (Tch), Aouzegueur (Ao), Edembo (Ed), Djanet (Dj); Shear zone and lineament names: Suture Zone East Saharan Craton (SZ ESC), West Ouzzal Shear Zone (WOSZ), East Ouzzal Shear Zone (EOSZ), Raghane Shear Zone (RSZ), Tin Amali Shear Zone (TASZ), 4°10’ Shear Zone, 4°50’ Shear Zone, 8°30’ Shear Zone.

Solid Earth Discuss., https://doi.org/10.5194/se-2018-50
Manuscript under review for journal Solid Earth
Discussion started: 27 June 2018

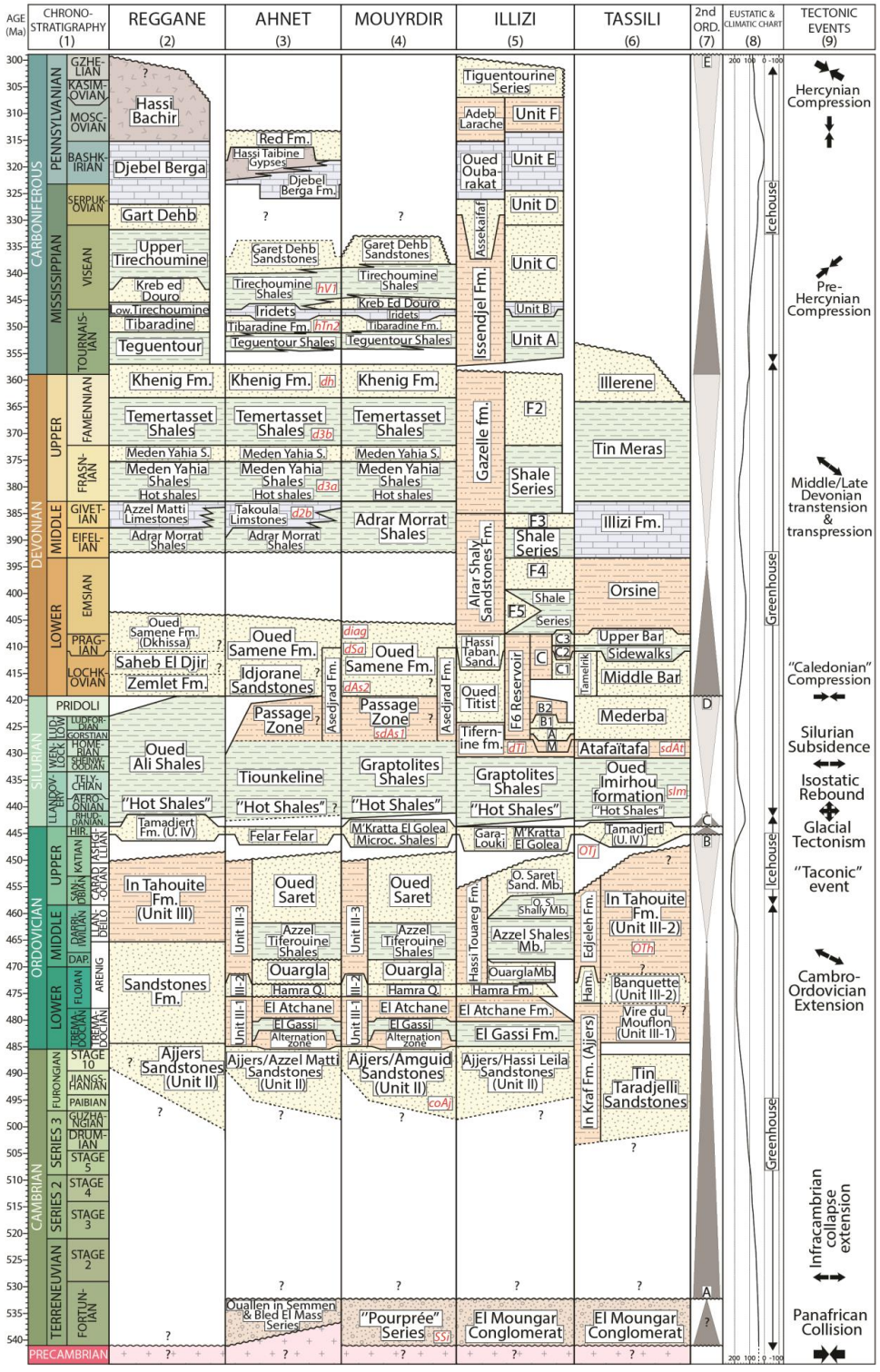

Solid Earth Discuss., https://doi.org/10.5194/se-2018-50
Manuscript under review for journal Solid Earth
Discussion started: 27 June 2018

1293 Figure 2: Paleozoic litho-stratigraphic, sequence stratigraphy and tectonic framework of the
1294 North Peri-Hoggar basins (North African Saharan Platform) compiled from (1)
1295 Chronostratigraphic chart (Ogg et al., 2016), (2) The Cambrian–Silurian (Askri et al., 1995)
1296 and the Devonian–Carboniferous stratigraphy of the Reggane basin (Cózar et al., 2016;
1297 Lubeseder, 2005; Lubeseder et al., 2010; Magloire, 1967; Wendt et al., 2006), (3) The
1298 Cambrian–Silurian (Paris, 1990; Wendt et al., 2006) and the Devonian–Carboniferous
1299 stratigraphy of the Ahnet basin (Beuf et al., 1971; Conrad, 1984, 1973; Legrand-Blain, 1985;
1300 Wendt et al., 2009b, 2006), (4) The Cambrian–Silurian (Askri et al., 1995; Paris, 1990; Videt
1301 et al., 2010) and the Devonian–Carboniferous stratigraphy of the Mouydir basin (Askri et al.,
1302 1995; Beuf et al., 1971; Conrad, 1984, 1973; Wendt et al., 2009b, 2006), (5) The Cambrian–
1303 Silurian (Eschard et al., 2005; Fekirine and Abdallah, 1998; Jardiné and Yapaudjian, 1968;
1304 Videt et al., 2010) and the Devonian–Carboniferous stratigraphy of the Illizi basin (Eschard et
1305 al., 2005; Fekirine and Abdallah, 1998; Jardiné and Yapaudjian, 1968), (6) The Cambrian–
1306 Silurian (Dubois, 1961; Dubois and Mazelet, 1964; Eschard et al., 2005; Henniche, 2002;
1307 Videt et al., 2010) and the Devonian–Carboniferous stratigraphy of the Tassili-N-Ajjers
1308 (Dubois et al., 1967; Eschard et al., 2005; Henniche, 2002; Wendt et al., 2009b), (7) Sequence
1309 stratigraphy of the Saharan Platform (Carr, 2002; Eschard et al., 2005; Fekirine and Abdallah,
1310 1998), (8) Eustatic and climatic chart (Haq and Schutter, 2008; Scotese et al., 1999), (9)
1311 Tectonic events (Boudjema, 1987; Coward and Ries, 2003; Craig et al., 2006; Guiraud et al.,
1312 2005; Lüning, 2005); (A) Infra-Tassilian (Pan-African) unconformity, (B) Taconic and glacial
1313 unconformity, (C) Isostatic rebound unconformity, (D) Caledonian unconformity, (E)
1314 Hercynian unconformity.
1315

Solid Earth Discuss., https://doi.org/10.5194/se-2018-50
Manuscript under review for journal Solid Earth
Discussion started: 27 June 2018

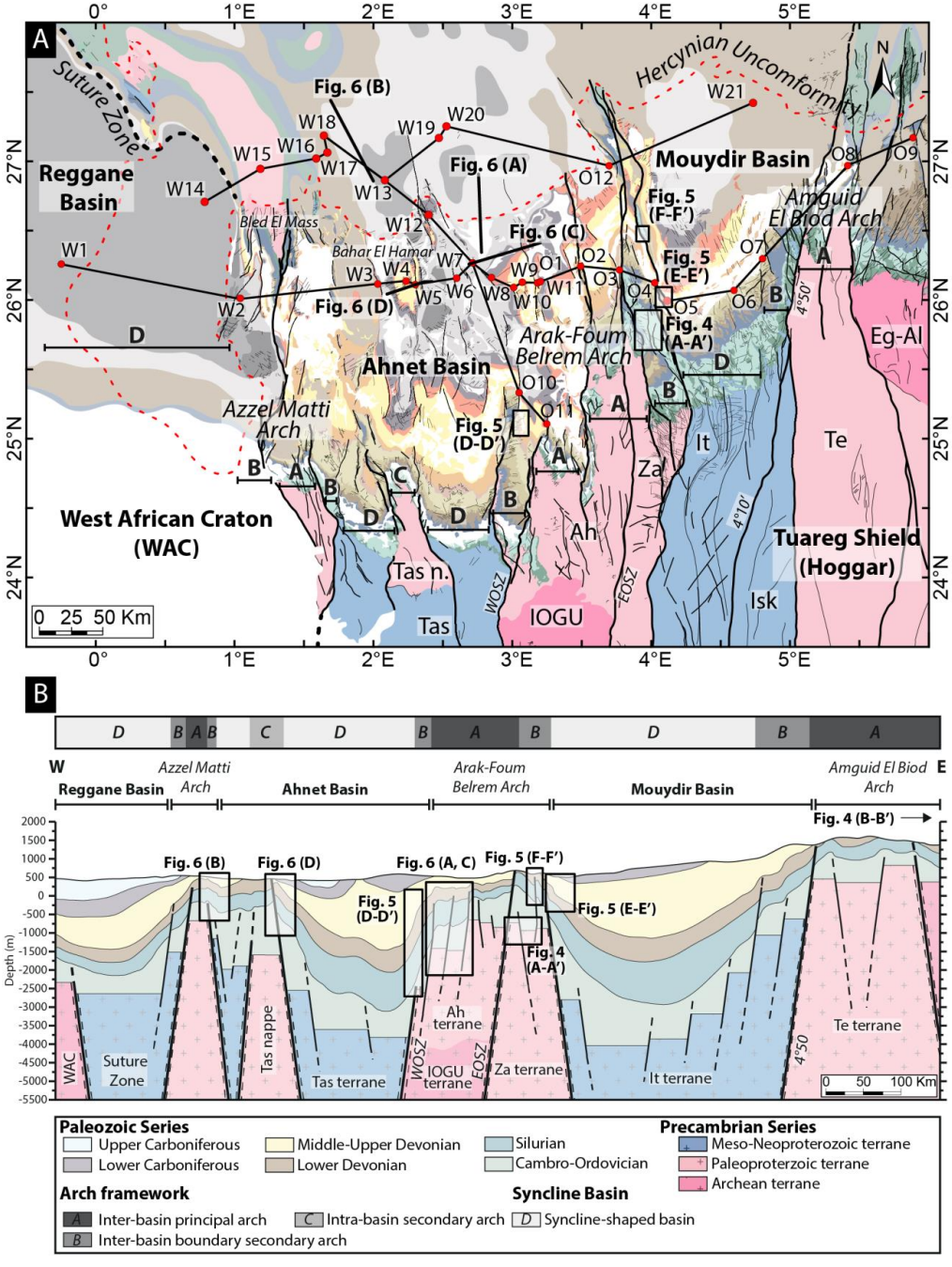

Figure 3: (A) Geological map of the Paleozoic of the Reggane, Ahnet, and Mouydir basins. Legend and references see Fig. 1. A: Inter-basin principal arch, B: Inter-basin boundary

Solid Earth Discuss., https://doi.org/10.5194/se-2018-50
Manuscript under review for journal Solid Earth
Discussion started: 27 June 2018

1319 secondary arch, C: Intra-basin secondary arch, D: Syncline-shaped basin. (B) E–W cross-
1320 section of the Reggane, Ahnet, and Mouydir basins associated with the different terranes and
1321 highlighting the classification of the different structural units (A: Inter-basin principal arch, B:
1322 Inter-basin boundary secondary arch, C: Intra-basin arch, D: Syncline-shaped basin).
1323 Localization of the interpreted sections (seismic profiles and satellite images). See figure 1 for
1324 location of the geological map A and cross section B.

1325

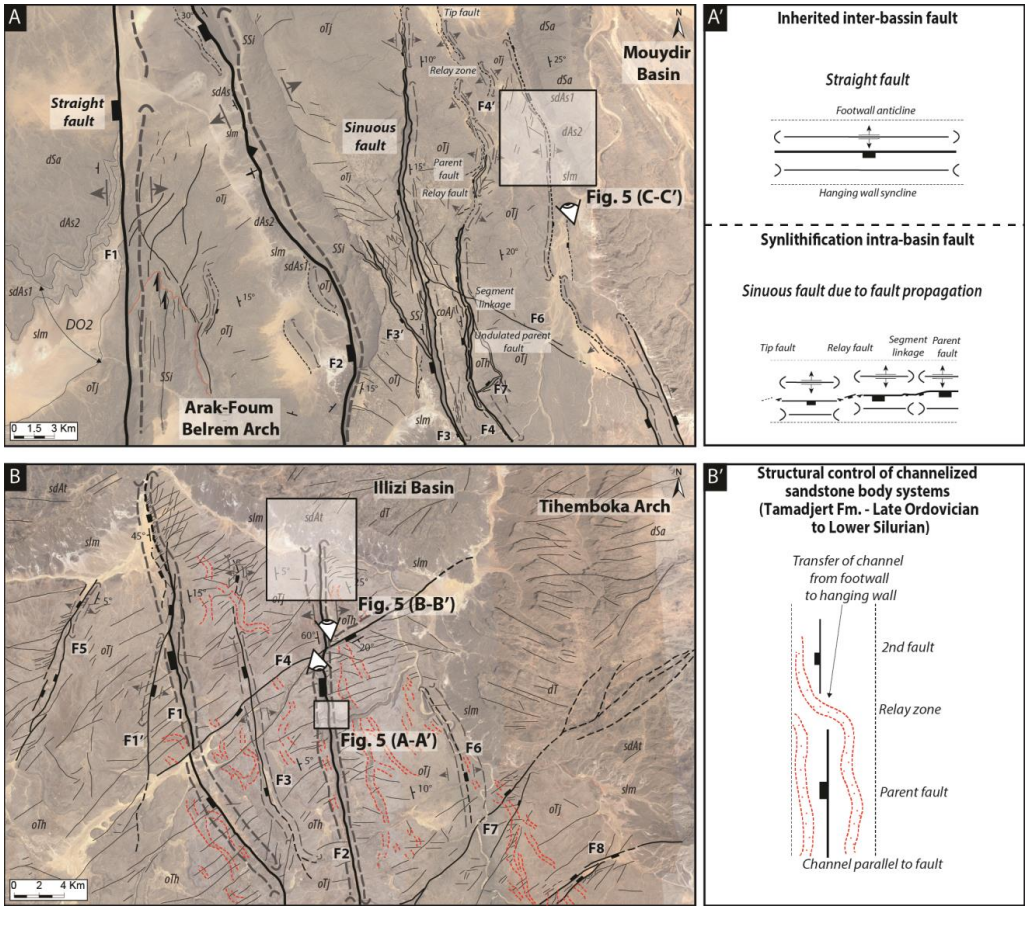

1326

1327 Figure 4: (A) Google Earth satellite images structural interpretation of the Djebel Settaf
1328 (Arak-Foum Belrem arch; inter-basin boundary secondary arch between the Ahnet and

Mouydir basins) of the Cambrian–Ordovician series showing straight and sinuous normal faults; (A') Typology of different types of faults (inherited straight faults vs sinuous short synlithification propagation faults). (B) Google Earth satellite images structural interpretation normal fault propagation in Cambrian–Ordovician series of South Adrar Assaouatene, Tassili-N-Ajjers (Tihemboka inter-basin boundary secondary arch between the Illizi and Murzuq basins); (B') Schematic model of structural control of channelized sandstone bodies. Dotted red line: Tamadjert Fm. channelized sandstone bodies. *OTh*: In Tahouite Fm (Early to Late Ordovician, Floian to Katian), *OTj*: Tamadjert Fm (Late Ordovician, Hirnantian), *sIm*: Imirhou Fm (Early Silurian), *sdAs1*: Asedjrad Fm 1 (Late Silurian to Early Devonian), *dAs2*: Asedjrad Fm 2 (Early Devonian, Lochkovian), *dSa*: Oued Samene Fm (Lower Devonian, Pragian). See Fig. 3 for map and cross-section location.

Solid Earth Discuss., https://doi.org/10.5194/se-2018-50
Manuscript under review for journal Solid Earth
Discussion started: 27 June 2018

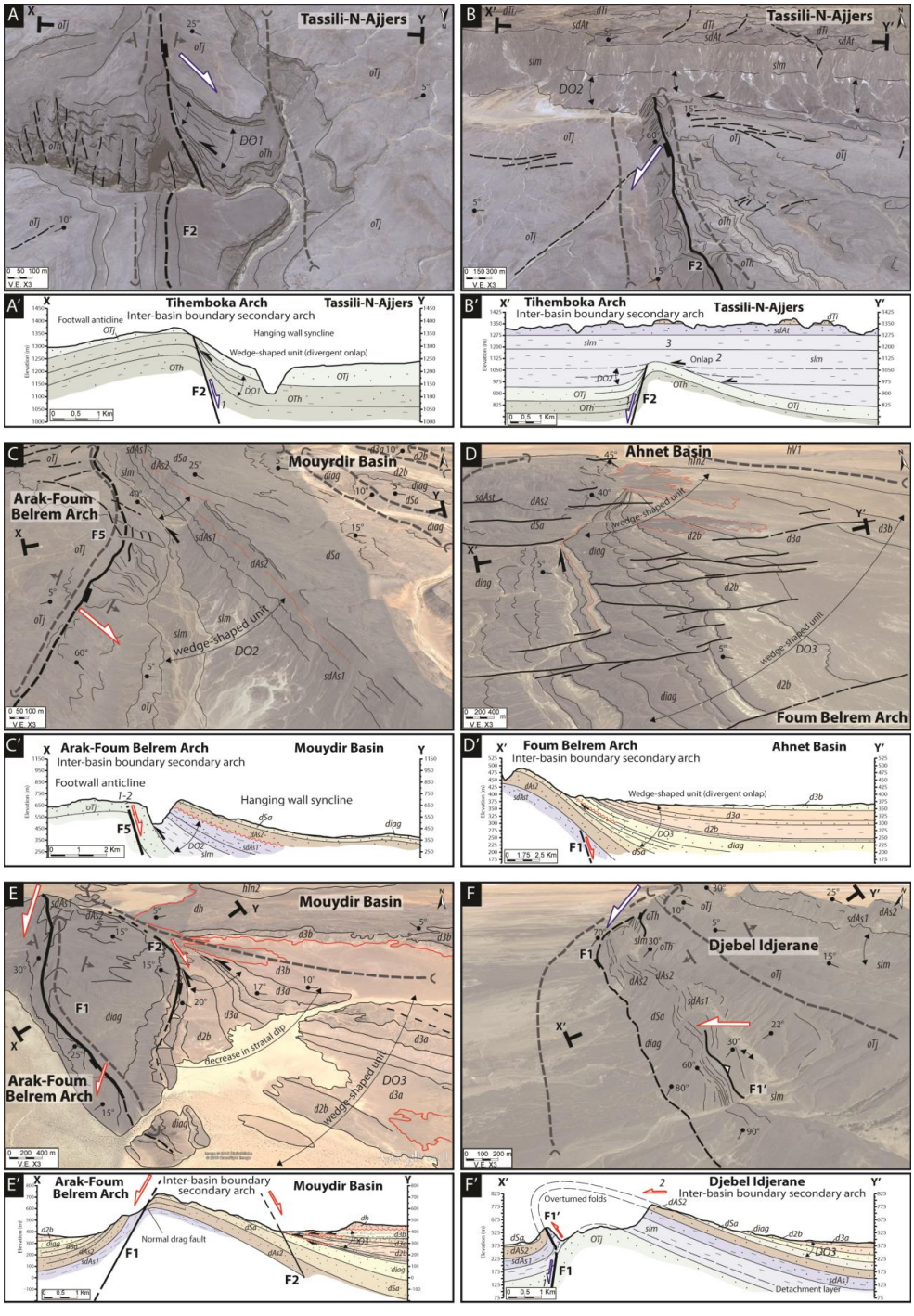

Figure 5: (A) Google Earth satellite images structural interpretation of South Adrar Assaouatene, Tassili-N-Ajjers (Tihemboka inter-basin boundary secondary arch between the Illizi and Murzuq basins) showing a normal fault (F2) associated with a footwall anticline and a hanging wall syncline with divergent onlaps (i.e. wedge-shaped unit DO1) in the In Tahouite series; (A') Cross-section between XY. 1: Cambrian–Ordovician extension during the deposition of In Tahouite series (Early to Late Ordovician). See fig. 4B for location. (B) Google Earth satellite images structural interpretation of North Adrar Assaouatene, Tassili-N-Ajjers (Tihemboka inter-basin boundary secondary arch between the Illizi and Murzuq basins) showing an ancient normal fault F2 escarpment reactivated and sealed during Silurian deposition (poly-historic paleo-reliefs) linked to thickness variation, divergent onlaps (DO2) in the hanging wall synclines, and onlaps on the fold hinge anticline; (B') Cross-section between X'Y'. 1: Early to Late Ordovician extension, 2: Late Ordovician to Early Silurian extension, 3: Middle to Late Silurian sealing (horizontal drape). See fig. 4B for location. (C) Google Earth satellite images structural interpretation of Dejbel Settaf (Arak-Foum Belrem arch; inter-basin boundary secondary arch between the Mouydir and Ahnet basins) showing a normal fault (F5) associated with forced fold with divergent strata (syncline-shaped hanging wall syncline and associated wedge-shaped unit DO2) and truncation in Silurian–Devonian series; (C') Cross-section between XY. 1: Cambrian–Ordovician extension, 2: Silurian–Devonian extensional reactivation (Caledonian extension). Red line: Unconformity. See fig. 4A for location. (D) Google Earth satellite images structural interpretation in the Ahnet basin (Arak-Foum Belrem arch; inter-basin boundary secondary arch between the Mouydir and Ahnet basins) showing blind basement normal fault (F1) associated with forced fold with in the hanging wall syncline divergent onlaps of Lower to Upper Devonian series (wedge-shaped unit DO3) and intra-Emsian truncation; (D') Cross-section between X'Y'. (E) Google Earth satellite images structural interpretation in the Mouydir basin (near Arak-Foum Belrem

arch, eastward inter-basin boundary secondary arch) showing N170° normal blind faults F1 and F2 forming a horst-graben system associated with forced fold with Lower to Upper Devonian series divergent onlaps (wedge-shaped unit DO3) and intra-Emsian truncation in the hanging-wall syncline; (E') Cross-section between XY. (F) Google Earth satellite images structural interpretation of Djebel Idjerane in the Mouydir basin (Arak-Foum Belrem arch, eastwards inter-basin boundary secondary arch) showing an inherited normal fault F1 transported from footwall to hanging wall associated with inverse fault F1' and accommodated by a detachment layer in Silurian shales series (Thickness variation of Imirhou Fm between footwall and hanging wall) and spilled dip strata markers of overturned folding; (F') Cross-section between X'Y'. 1: Cambrian–Ordovician extension, 2: Middle to Late Devonian compression. *OTh*: In Tahouite Fm (Early to Late Ordovician, Floian to Katian), *OTj*: Tamadjert Fm (Late Ordovician, Hirnantian), *sIm*: Imirhou Fm (Early to Mid Silurian), *sdAt*: Atafaïtafa Fm (Middle Silurian), *dTi*: Tifernine Fm (Middle Silurian), *sdAs1*: Asedjrad Fm 1 (Late Silurian to Early Devonian), *dAs2*: Asedjrad Fm 2 (Early Devonian, Lochkovian), *dSa*: Oued Samene Fm (Early Devonian, Pragian), *diag*: Oued Samene shaly-sandstones Fm (Early Devonian, Emsian?), *d2b*: Givetian, *d3a*: Meden Yahia Fm (Late Devonian, Frasnian), *d3b*: Meden Yahia Fm (Late Devonian, Famennian), *dh*: Khenig sandstones (late Famennian to early Tournaisian), *hTn2*: late Tournaisian, *hV1*: early Visean. See Figs. 1 and 3 for map and cross-section location.

Solid Earth Discuss., https://doi.org/10.5194/se-2018-50
Manuscript under review for journal Solid Earth
Discussion started: 27 June 2018

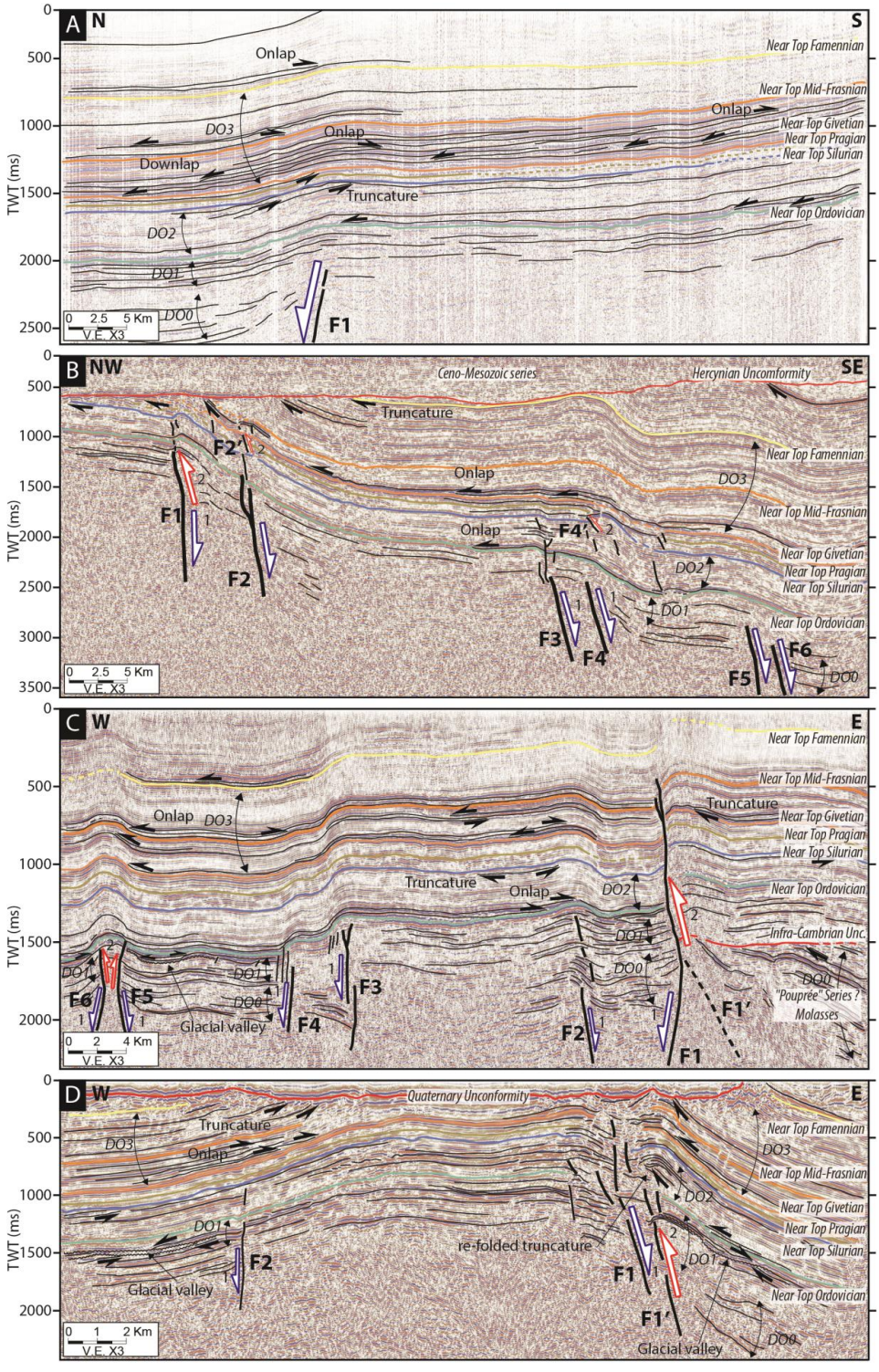

Solid Earth Discuss., https://doi.org/10.5194/se-2018-50
Manuscript under review for journal Solid Earth
Discussion started: 27 June 2018

Figure 6: (A) N–S interpreted seismic profile in the Ahnet basin near Erg Tegunentour (near Arak-Foum Belrem arch, westward inter-basin boundary secondary arch) showing steeply-dipping northward basement normal blind faults associated with forced folding. Strata lapout geometries shows Lower Silurian onlaps on the top Ordovician, Upper Silurian and Lower Devonian truncations, onlaps and dowlaps of Frasnian series on top Givetian unit and onlap near top Famennian. (B) NW–SE interpreted seismic profile of near Azzel Matti arch (inter-basin principal arch) showing steeply-dipping south-eastwards basement normal blind faults associated with forced folds. The westernmost structures are featured by reverse fault related propagation fold. Strata lapout geometries show Silurian onlaps on top Ordovician, Frasnian onlaps, thinning of Frasnian and Silurian series near the arch; truncation of Paleozoic series by Mesozoic unit on Hercynian unconformity. (C) W–E interpreted profile of the Ahnet basin (Arak-Foum Belrem arch, westward inter-basin boundary secondary arch) showing horst and graben structures influencing Paleozoic tectonics associated with forced folds. Strata lapout geometries show Precambrian basement tilted structure overlain by Cambrian–Ordovician angular unconformity, incised valley in the Ordovician series, Silurian onlaps on top Ordovician, Silurian onlaps on top Ordovician, Silurian–Devonian truncation, Frasnian onlaps on top Givetian and near top Famennian onlaps. (D) W–E interpreted seismic profile of Bahar el Hammar in the Ahnet basin (Ahnet intra-basin secondary arch) showing steeply-dipping normal faults F1 and F2 forming a horst positively inverted associated with folding. Strata lapout geometries show glacial valley in the Ordovician series, Silurian onlaps on top Ordovician, Silurian onlaps on top Ordovician; Silurian–Devonian truncation re-folded, Frasnian onlaps on top Givetian. Multiple activation and inversion of normal faults are correlated to divergent onlaps (wedge-shaped units): DO0, Infra-Cambrian extension, DO1 Cambrian–Ordovician extension, DO2 Silurian extension with local Silurian–Devonian positive inversion, and DO3 Frasnian–Famennian extension-local compression (transported

Solid Earth Discuss., https://doi.org/10.5194/se-2018-50
Manuscript under review for journal Solid Earth
Discussion started: 27 June 2018

1413 fault with a tectonic transport from footwall to hanging wall). See figure 3 for map and cross-
1414 section location.

1415

Solid Earth Discuss., https://doi.org/10.5194/se-2018-50
Manuscript under review for journal Solid Earth
Discussion started: 27 June 2018

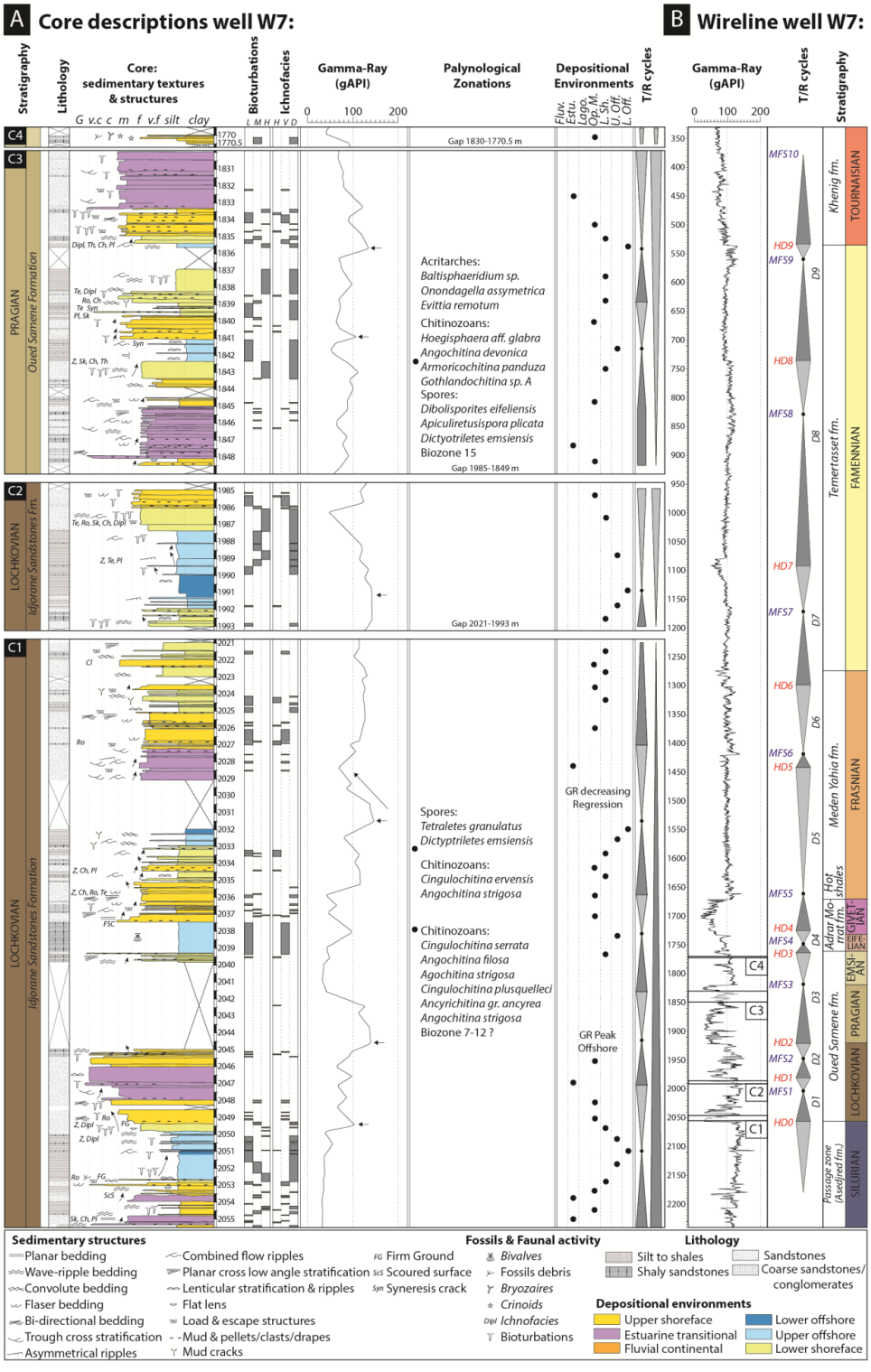

Solid Earth Discuss., https://doi.org/10.5194/se-2018-50
Manuscript under review for journal Solid Earth
Discussion started: 27 June 2018

1417 Figure 7: Core description, palynological calibration and gamma-ray signatures of well W7
1418 modified from internal core description report (Dokka, 1999) and internal palynological
1419 report (Azzoune, 1999). For location of well W7 see figure 3A. Lithological and
1420 sedimentological studies were synthetized from internal Sonatrach (Dokka, 1999), IFP reports
1421 (Eschard et al., 1999), and published articles (Beuf et al., 1971; Biju-Duval et al., 1968;
1422 Wendt et al., 2006). Biozonations from Magloire (1967) and Boumendjel et al. (1988) are
1423 based on palynological data from internal unpublished data (wells W1, W7, W12 W13, W19,
1424 and W20 in Figs. 9, 10 supplementary data 3; Abdesselam-Rouighi, 1991; Azzoune, 1999;
1425 Khiar, 1974). Well W18 is supported by palynological data and biozonations from Hassan
1426 Kermandji et al. (2008).

Solid Earth Discuss., https://doi.org/10.5194/se-2018-50
Manuscript under review for journal Solid Earth
Discussion started: 27 June 2018

Criteria & characteristics					Depositional environments	
Facies associations	Textures/Lithology	Sedimentary structures	Biotic/non biotic grains	Ichnofacies		
AF1	Conglomerates, mid to coarse sandstones, siltstones, shales	Trough cross-bedding, mud clasts, lag deposits, fluidal and overturn structures, imbricated grains, lenticular laminations, oblique stratification	Rare oolitic intercalations, imbricated pebbles, sandstones, ironstones, phosphorites, corroded quartz grains, calcareous matrix, brachiopod coquinas, phosphatized pebbles, hematite, azurite, quartz	Rare bioturbation	Fluvial	Continental (Fluvial)
AF2	Silt to argillaceous fine sandstone	Current ripples, climbing ripples, crevasse splay, root traces, paleosols, plant debris	Nodules, ferruginous horizon		Flood plain	
AF3a	Fine to coarse sandstones, argillaceous siltstones, shales (heterolithic)	Trough cross-bedding, some planar bedding, flaser bedding, mud clasts, mud drapes, root trace, desiccation cracks, water escape, wavy bedding, shale pebble, sigmoidal cross-bedding	Brachiopods, trilobites, tentaculites graptolites	Bioturbations, *Skolithos* (Sk), *Planolites*, (Pl)	Delta/Estuarine channels	Coastal Plain (Transitional Marine/Continental)
AF3b	Very coarse-grained poorly sorted sandstone	Trough cross-bedding, sigmoidal cross-bedding, abundant mud clasts and mud drapes		Increasing upward bioturbation *Skolithos* (Sk)	Fluvial/Tidal distributary channels	
AF3c	Fine-grained to very coarse-grained heterolithic sandstone	Sigmoidal cross-bedding with multidirectional tidal bundles, wavy, lenticular, flaser bedding, occasional current and oscillation ripples, occasional mud cracks		Intense bioturbation, *Skolithos* (Sk), *Planolites*, (Pl), *Thalassinoides* (Th)	Tidal sand flat	
AF3d	Mudstones, varicolored shales, thin sandstone layers	Occasional wave ripples, mud cracks, horizontal lamination, rare multi-directional ripples	Absence of ammonoids, goniatites, calymenids, pelecypod molds, brachiopods coquinas	Intense bioturbation, *Skolithos* (Sk), *Planolites*, (Pl), *Thalassinoides* (Th)	Lagoon/Mudflat	
AF4a	Silty mudstone associated with coarse to very coarse argillaceous sandstone, poorly sorted, heterolithic silty mudstone	Sigmoidal cross-bedding, abundant mud clasts, wavy, lenticular cross-bedding and flaser bedding, abundant current and oscillation ripples, mud drapes	Shell debris (crinoids, brachiopods)	Strongly bioturbated *Skolithos* (Sk), *Planolites*, (Pl)	Subtidal	Shoreface
AF4b	Fine to mid grained sandstones interbedded with argillaceous siltstone and mudstone, bioclastic carbonates sandstones, brownish sandstones and clays, silts	Oscillation ripples, swaley cross-bedding, bidirectional bedding, flaser bedding, rare hummocky cross-bedding, mud cracks (syneresis), convolute bedding, wavy bedding, combined flow ripples, planar cross low angle stratification, cross-bedding, ripple marks, centimetric bedding, shale pebbles	Ooids, crinoids, bryozoans, coral clasts, fossil debris, stromatoporoids, tabulates, colonial rugose corals, myriad pelagic styliolinids, neritic tentaculitids, brachiopods, iron ooliths, abundant micas	*Skolithos* (Sk), *Cruziana*, *Planolites*, (Pl) *Chondrites* (Ch), *Teichichnus* (Te), *Spirophytons* (Sp)	Open marine-upper shoreface	
AF4c	Silty shales to fine sandstones (heterolithic)	Hummocky cross-bedding, planar bedding, combined flow ripples, convolute bedding, dish structures, mud drapes, remnant ripples, flat lenses, slumping	Intense bioturbation, *Cruziana*	*Thalassinoides* (Th), *Planolites* (Pl), *Skolithos* (Sk), *Diplocraterion* (Dipl), *Teichichnus* (Te), *Chondrites* (Ch), *Rogerella* (Ro), *Climactichnites* (Cl)	Lower shoreface	
AF5a	Grey silty-shales, bundles of skeletal wackestones, silty greenish shale interlayers fine grained sandstones, calcareous mudstones, black shales, polychrome clays (black, brown, grey, green, red, pink), grey and reddish shales	Lenticular sandstones, rare hummocky cross-bedding, mud mounds, mud buildups, low-angle cross-bedding, tempestite bedding, slumping, deep groove marks	Intensive burrowing, bivalve debris, horizontal burrows, skeletal remains (goniatites, orthoconic, nautiloids, styliolinids, trilobites, crinoids, solitary rugose, corals, limestones nodules, ironstone nodules and layers	*Zoophycos* (Z), *Teichichnus* (Te), *Planolites* (Pl)	Upper offshore	Offshore
AF5b	Black silty-shales (mudstones), bituminous mudstones-wackestones, packstones	Rare structures	parallel-aligned styliolinids, gonitaties, orthoconic nautiloids, pelagic pelecypod *Buchiola*, anoxic conditions, limestone nodules, goniatites, *Buchiola*, *tentaculitids*, ostracods and rare fish remains, *Tornoceras*, *Aulatornoceras*, *Lobotornoceras*, *Manticoceras*, *Costamanticoceras* and *Virginoceras*, graptolites	*Zoophycos* (Z)	Lower offshore	

Solid Earth Discuss., https://doi.org/10.5194/se-2018-50
Manuscript under review for journal Solid Earth
Discussion started: 27 June 2018

1427 Table 1: Synthesis of facies associations (AF1 to AF5), depositional environments, and
1428 electrofacies in the Devonian series compiled from internal (Eschard et al., 1999) and
1429 published studies (Beuf et al., 1971; Biju-Duval et al., 1968; Wendt et al., 2006).

1430

Solid Earth Discuss., https://doi.org/10.5194/se-2018-50
Manuscript under review for journal Solid Earth
Discussion started: 27 June 2018

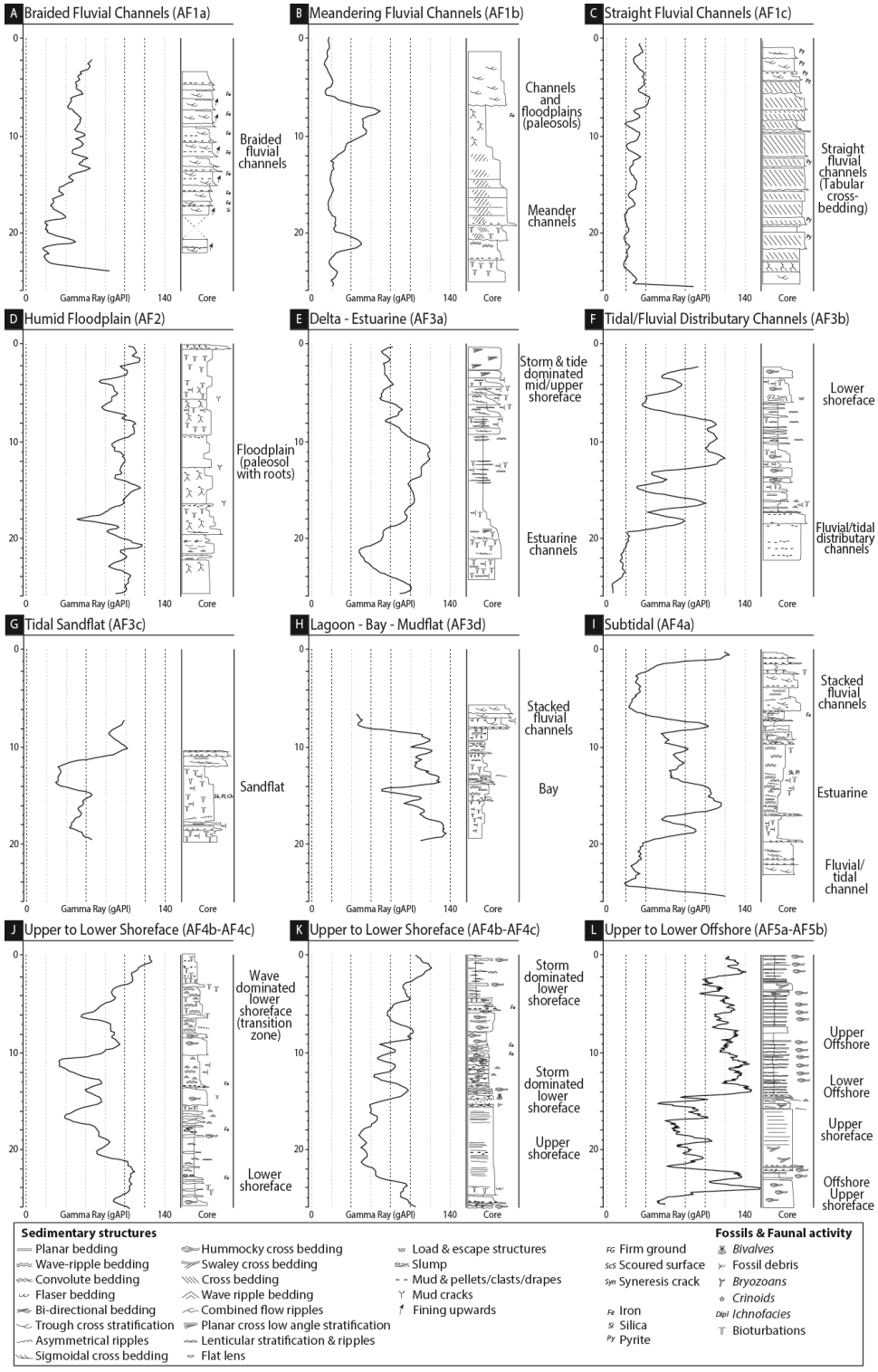

Solid Earth Discuss., https://doi.org/10.5194/se-2018-50
Manuscript under review for journal Solid Earth
Discussion started: 27 June 2018

1432 Figure 8: The main depositional environments (A to L) and their associated electrofacies (i.e.
1433 gamma-ray patterns) modified and compiled from Eschard et al., (1999).

1434

Solid Earth Discuss., https://doi.org/10.5194/se-2018-50
Manuscript under review for journal Solid Earth
Discussion started: 27 June 2018

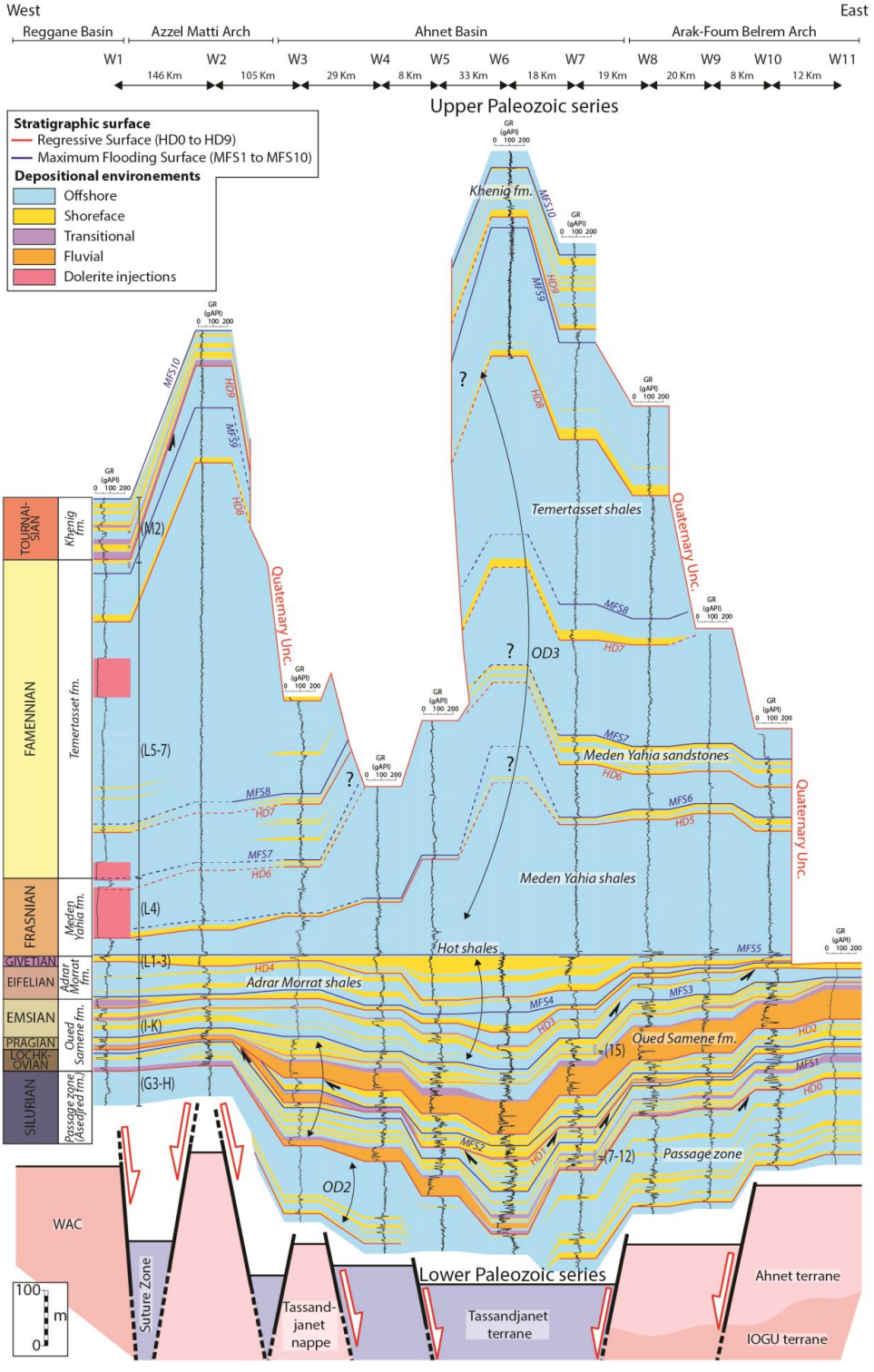

Solid Earth Discuss., https://doi.org/10.5194/se-2018-50
Manuscript under review for journal Solid Earth
Discussion started: 27 June 2018

1436 Figure 9: SE–W cross-section between the Reggane basin, Azzel Matti arch, Ahnet basin,
1437 Arak-Foum Belrem arch, Mouydir basin, and Amguid El Biod arch (well locations in fig. 3).
1438 Well W1 biozone calibration from Hassan, (1984) internal report is based on Magloire's
1439 (1967) classification: biozone G3-H (Wenlock–Ludlow, Upper Silurian), biozone I-K
1440 (Lochkovian–Emsian, Lower Devonian), biozone L1-3 (Eifelian–Givetian, Middle
1441 Devonian), biozone L4 (Frasnian, Upper Devonian), biozone L5-7 (Famennian, Upper
1442 Devonian), biozone M2 (Tournaisian–Lower Carboniferous). Well W7 biozone calibration
1443 from Azzoune's (1999) internal report is based on Boumendjel's (1987) classification:
1444 biozone 7-12 (Lochkovian, Lower Devonian), biozone 15 (Emsian, Lower Devonian).
1445 Interpretation of the basement is based on Figs. 1, 3 and supplementary data 4. Outcrop
1446 location is in Fig. 3.

1447

Solid Earth Discuss., https://doi.org/10.5194/se-2018-50
Manuscript under review for journal Solid Earth
Discussion started: 27 June 2018

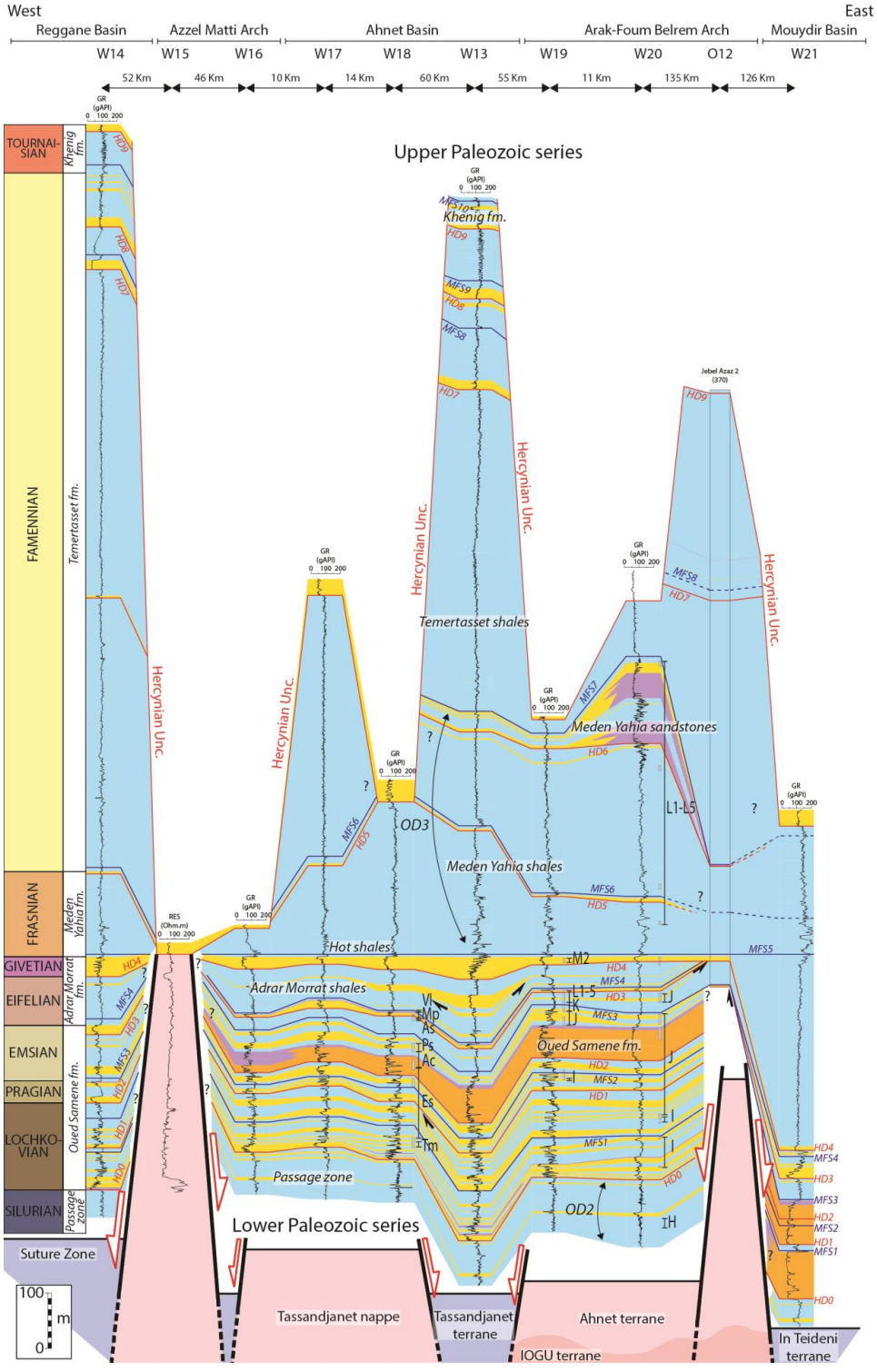

Figure 10: NE–W cross-section between the Reggane basin, Azzel Matti arch, Ahnet basin, Arak-Foum Belrem arch, Mouydir basin, and Amguid El Biod arch (well locations in fig. 3). Well W18 biozone calibration is based on Kermandji et al. (2009): biozone (Tm) *tidikeltense microbaculatus* (Lochkovian, Lower Devonian), biozone (Es) *emsiensis spinaeformis* (Lochkovian-Pragian, Lower Devonian), biozone (Ac) *arenorugosa caperatus* (Pragian, Lower Devonian), biozone (Ps) *poligonalis subgranifer* (Pragian–Emsian, Lower Devonian), biozone (As) *annulatus svalbardiae* (Emsian, Lower Devonian), biozone (Mp) *microancyreus protea* (Emsian–Eifelian, Lower to Middle Devonian), biozone (Vl) *velatus langii* (Eifelian, Middle Devonian). Well W19 and W20 biozones calibration from internal reports (Abdesselam-Rouighi, 1991; Khiar, 1974) is based on Magloire's (1967) classification: biozone H (Pridoli, Upper Silurian), biozone I (Lochkovian, Lower Devonian), biozone J (Pragian, Lower Devonian), biozone K (Emsian, Lower Devonian), biozone L1-5 (Middle Devonian to Upper Devonian). Interpretation of the basement is based on Figs. 1, 3 and supplementary data 4. Outcrop location is in Fig. 3.

Solid Earth Discuss., https://doi.org/10.5194/se-2018-50
Manuscript under review for journal Solid Earth
Discussion started: 27 June 2018

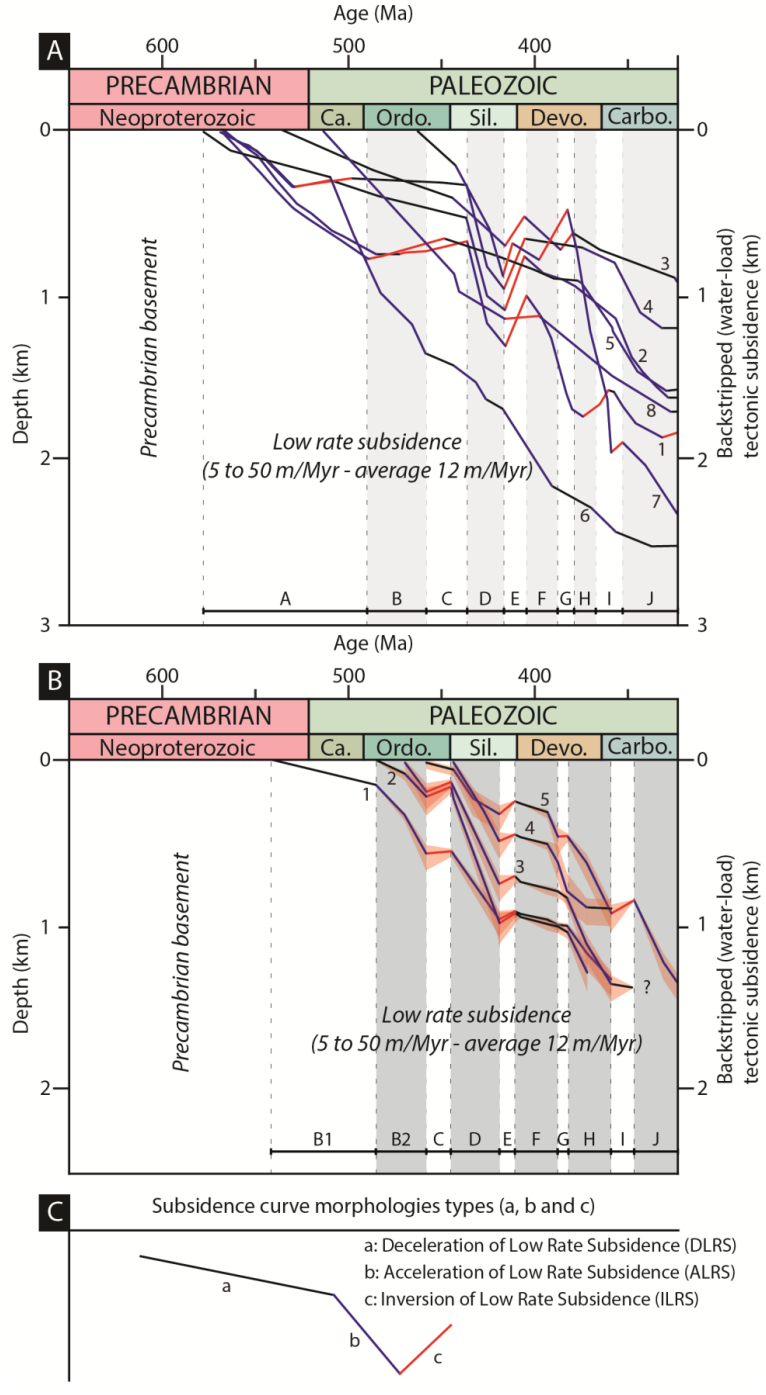

Figure 11: (A) Tectonic backstripped curves of the Paleozoic North Saharan Platform (peri-Hoggar basins) compiled from literature (1: HAD-1 well in Ghadamès basin (Makhous and Galushkin, 2003a); 2: Well RPL-101 in Reggane basin (Makhous and Galushkin, 2003a); 3: L1-1 well in Murzuq basin (Galushkin and Eloghbi, 2014); 4: TGE-1 in Illizi basin (Makhous and Galushkin, 2003b); 5: REG-1 in Timimoun basin (Makhous and Galushkin, 2003a); 6: Ghadamès-Berkine basin (Allen and Armitage, 2011; Yahi, 1999); 7: well in Sbâa basin (Tournier, 2010); 8: well B1NC43 in Al Kufrah basin (Holt et al., 2010). (B) Tectonic backstripped curves of wells in the study area (1: well W17 in Ahnet basin; 2: well W5 in Ahnet basin; 3: well W7 in Ahnet basin; 4: well W21 in Mouydir basin; 5: well W1 in Reggane basin); (C) The data show low rate subsidence with periods of deceleration (Deceleration of Low Rate Subsidence: DLRS), acceleration (Acceleration of Low Rate Subsidence: ALRS), or inversion (Inversion of Low Rate Subsidence: ILRS) synchronous and correlated with regional tectonic pulses (i.e. major geodynamic events). A: Late Pan-African compression and collapse (type a, b, and c subsidence), B: Undifferentiated Cambrian–Ordovician (type a, b, and c subsidence), B1: Cambrian–Ordovician tectonic quiescence (type a subsidence), B2: Cambrian–Ordovician extension (type b subsidence), C: Late Ordovician glacial and isostatic rebound (type c subsidence), D: Silurian extension (type b subsidence), E: Late Silurian Caledonian compression (type c subsidence), F: Early Devonian tectonic quiescence (type a subsidence), G-H: Middle to late Devonian extension with local compression (i.e. inversion structures, type b and c subsidence), I: Early Carboniferous extension with local tectonic pre-Hercynian compression (type c and b subsidence), J: Middle Carboniferous tectonic extension (type b subsidence), K: Late Carboniferous–Early Permian Hercynian compression (type c subsidence).

Solid Earth Discuss., https://doi.org/10.5194/se-2018-50
Manuscript under review for journal Solid Earth
Discussion started: 27 June 2018

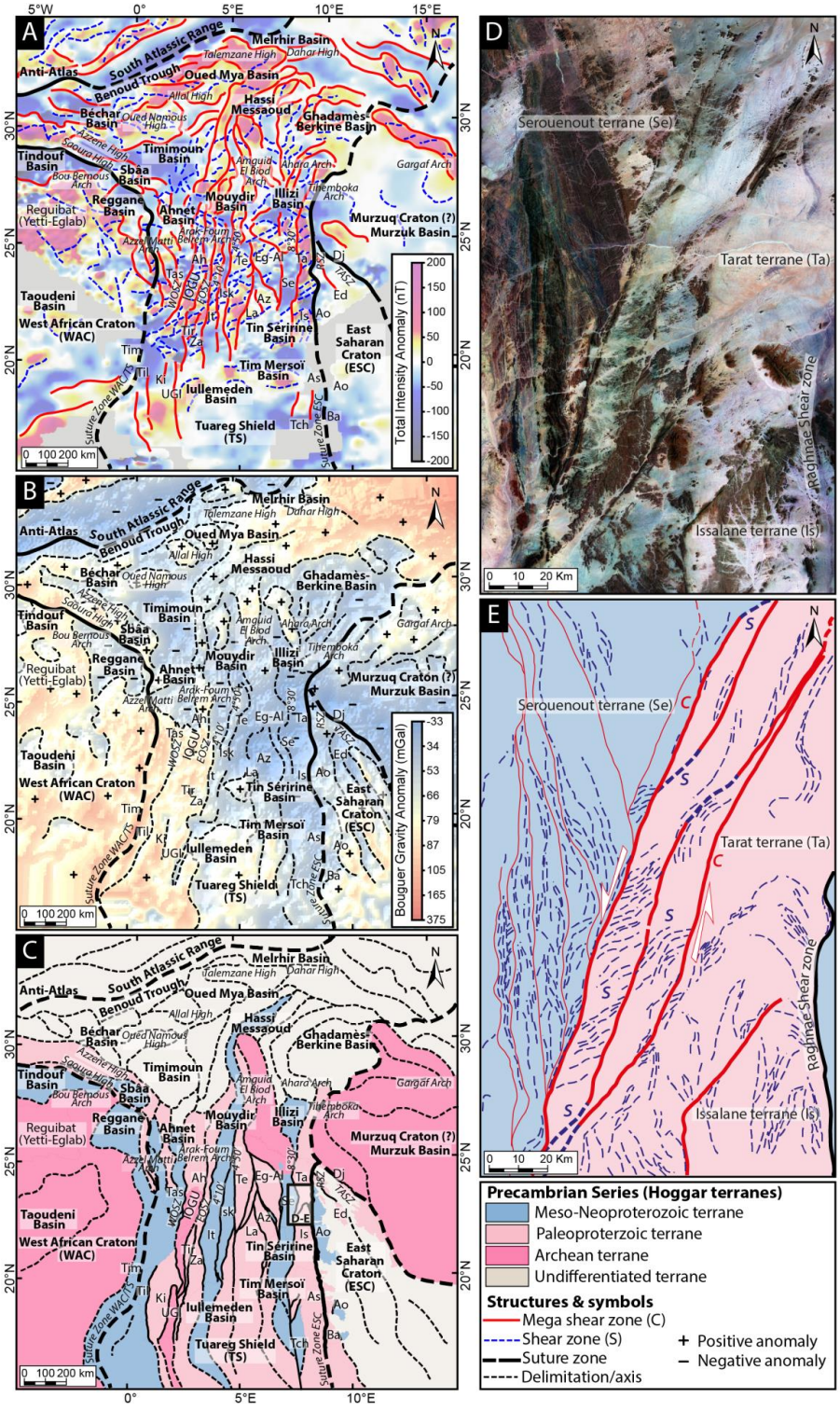

Solid Earth Discuss., https://doi.org/10.5194/se-2018-50
Manuscript under review for journal Solid Earth
Discussion started: 27 June 2018

1490 Figure 12: (A) Interpreted aeromagnetic anomaly map (https://www.geomag.us/) of the
1491 Paleozoic North Saharan Platform (peri-Hoggar basins) showing the different terranes
1492 delimited by NS, NW–SE and NE–SW lineaments and mega-sigmoid structures (SC shear
1493 fabrics); (B) Bouguer anomaly map (from International Gravimetric Bureau:
1494 http://bgi.omp.obs-mip.fr/) of North Saharan Platform (peri-Hoggar basins) presenting
1495 evidence of positive anomalies under arches and negative anomalies under basins; (C)
1496 Interpreted map of basement terranes according to their age (compilation of data sets in Fig. 1
1497 and supplementary data 4); (D) Satellite images (7ETM+ from USGS:
1498 https://earthexplorer.usgs.gov/) of Paleoproterozoic Issalane-Tarat terrane, Central Hoggar
1499 (see fig. 12C for location); (E) Interpreted satellite images of Paleoproterozoic Issalane-Tarat
1500 terrane showing sinistral sigmoid mega-structures associated with transcurrent lithospheric
1501 shear fabrics SC.

1502

Solid Earth Discuss., https://doi.org/10.5194/se-2018-50
Manuscript under review for journal Solid Earth
Discussion started: 27 June 2018

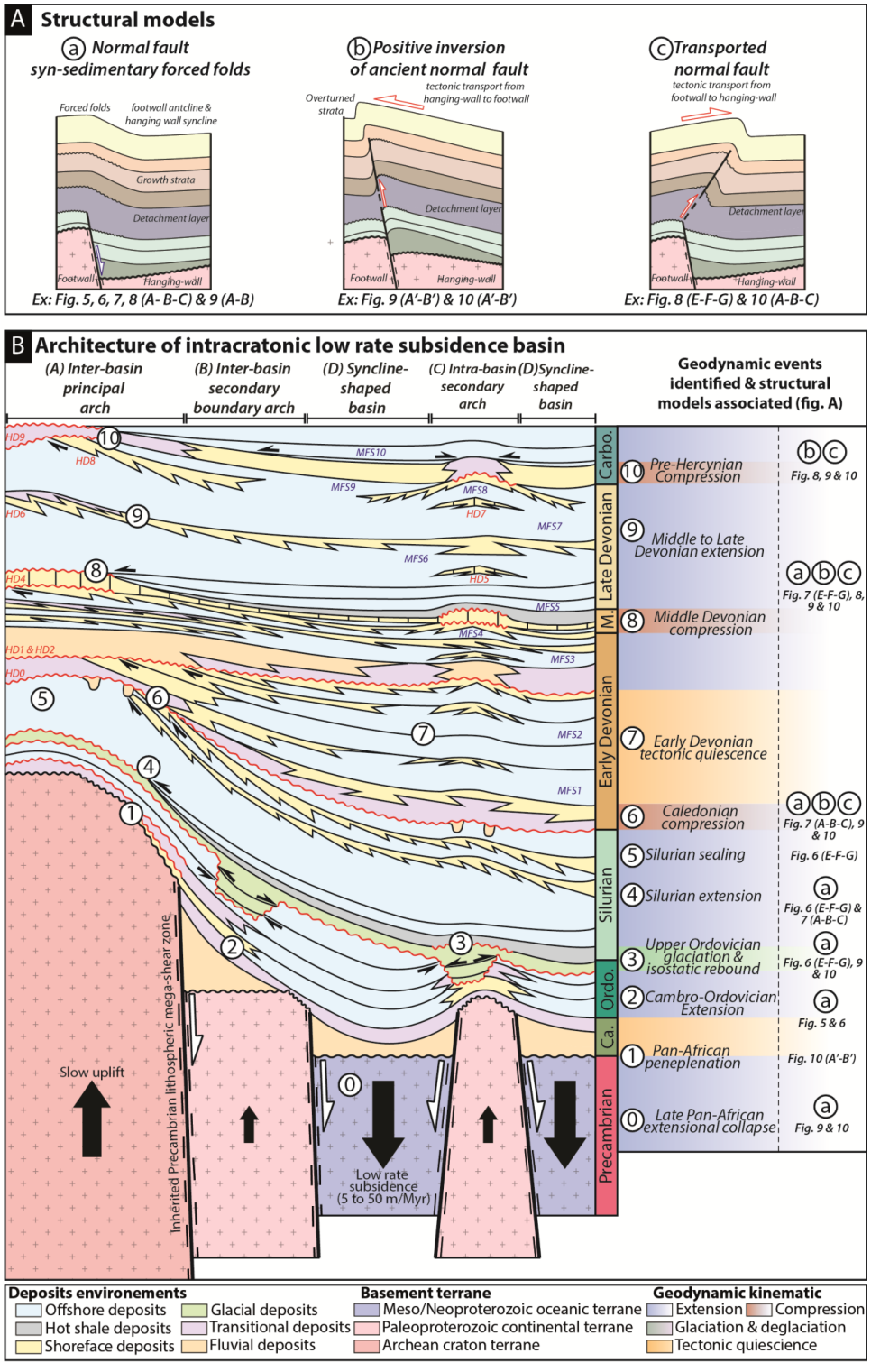

Solid Earth Discuss., https://doi.org/10.5194/se-2018-50
Manuscript under review for journal Solid Earth
Discussion started: 27 June 2018

1504 Figure 13: (A) Different structural model styles identified from the analysis of seismic
1505 profiles and from interpretation of the satellite images; (B) Conceptual model of the
1506 architecture of intracratonic low rate subsidence basin and synthesis of the tectonic kinematics
1507 during the Paleozoic. Note that the differential subsidence between arches and basins is
1508 controlled by terrane heterogeneity (i.e. thermo-chronologic age, rheology, etc.).